applied sciences

MDPI

Article

Spectral Analysis of Electromagnetic Diffraction Phenomena in Angular Regions Filled by Arbitrary Linear Media

Vito G. Daniele † and Guido Lombardi *,†

The Department of Electronics and Telecommunications (DET), Politecnico di Torino, 10129 Torino, Italy; vito.daniele@polito.it

* Correspondence: guido.lombardi@polito.it; Tel.: +39-011-0904012

† These authors contributed equally to this work.

Abstract: A general theory for solving electromagnetic diffraction problems with impenetrable/penetrable wedges immersed in/made of an arbitrary linear (bianistropic) medium is presented. This novel and general spectral theory handles complex scattering problems by using transverse equations for layered planar and angular structures, the characteristic Green function procedure, the Wiener–Hopf technique, and a new methodology for solving GWHEs. The technique has been proven effective for analyzing problems involving wedges immersed in isotropic media; in this study, we extend the theory to more general cases while providing all necessary mathematical tools and corresponding validations. We obtain generalized Wiener–Hopf equations (GWHEs) from spectral functional equations in angular regions filled by arbitrary linear media. The equations can be interpreted with a network formalism for a systematic view. We recall that spectral methods (such as the Sommerfeld–Malyuzhinets (SM) method, the Kontorovich–Lebedev (KL) transform method, and the Wiener–Hopf (WH) method) are well-consolidated, fundamental, and effective tools for the correct and precise analysis of electromagnetic diffraction problems constituted by abrupt discontinuities immersed in media with one propagation constant, although they are not immediately applicable to multiple-propagation-constant problems. To the best of our knowledge, the proposed mathematical technique is the first extension of spectral analysis to electromagnetic problems in the presence of angular regions filled by complex arbitrary linear media, thereby providing novel mathematical tools. Validation through fundamental examples is proposed.

Keywords: wave motion; diffraction; electromagnetism; arbitrary linear media; bianisotropic media; layered media; applied mathematics; Green's function; Wiener–Hopf method; integral equations; Fredholm factorization

Citation: Daniele, V.G.; Lombardi, G. Spectral Analysis of Electromagnetic Diffraction Phenomena in Angular Regions Filled by Arbitrary Linear Media. *Appl. Sci.* **2024**, *14*, 8685. https://doi.org/10.3390/app14198685

Academic Editor: Augusto Ferrante

Received: 21 July 2024
Revised: 19 August 2024
Accepted: 27 August 2024
Published: 26 September 2024

1. Introduction

The theory of wave diffraction constitutes one of the fundamental problems in mathematical physics. Apart from its direct relevance to engineering and physics, this subject gives rise to significant methodologies in applied mathematics.

Spectral methods play a crucial role in the study of electromagnetic diffraction. Notably, the Sommerfeld–Malyuzhinets (SM) method, the Kontorovich–Lebedev (KL) transform method, and the Wiener–Hopf (WH) method are fundamental and complementary in studying diffraction problems in the presence of sharp discontinuities. These methods have been extensively and effectively applied for studying wedge diffraction in isotropic regions; see [1–6] for SM, Refs. [7–10] for KL, and Refs. [11,12] for WH, along with the references therein starting from the early 2000s literature produced by the authors of this study. Moreover, using synergy among the three methods (WH, SM, and KL), the authors obtained a complete network representation of the angular region in the presence of isotropic media [13], which helped to build a systematic methodology for analysis.

The main advantage of the aforementioned techniques (SM and KL) is also a limitation, i.e., the utilization of the spectral complex angular plane derived from the Sommerfeld

integral theory [14], which, since the early 2000s, the authors of this study have also effectively used in the WH framework for Fredholm factorization [11,12] and in the definition of rotating waves in isotropic angular regions [11,12]. The definition of this complex plane is intricately connected to the physics of the problem, as it specifically requires spectral transformations associated with the propagation constant. Consequently, this methodology is applicable to problems involving a single propagation constant, such as isotropic media in electromagnetic fields, as well as other specific problem configurations with decoupling properties in propagation modalities. Different attempts have been developed to extend the spectral analysis to diffraction problems in more complex media, such as gyrotropic media and/or uniaxial media. For example, we recall the analysis of scattering by a perfect electrically conducting (PEC) half-plane immersed in such anisotropic media; see [15–24]. However, to the best of our knowledge no spectral method for scattering problems by wedges in arbitrary linear media (i.e., bianisotropic media [25–27]) characterized by multiple propagation constants has been developed to date. One of the most important results obtained in the presence of anisotropic media is the exact solution obtained by Felsen in the case of scattering by a PEC wedge immersed in a uniaxial medium illuminated by plane waves at normal incidence [17,18]. However, the method used for this problem is substantially that of the separation of variables after transformations in the physical domain, which does not present the powerful characteristics of spectral methods such as asymptotic evaluation of fields and physical interpretation of field components in terms of structural and source spectral singularities. Other important works have examined the behavior of the field near the edge of a wedge immersed in a complex medium [28] and diffraction by a wedge immersed in the special case of an isotropic chiral medium with the SM method [29].

Given our experience in spectral analysis of complex electromagnetic scattering problems in isotropic media [11,12,30–32], and with the help of the theory proposed in [33] for the analysis of structures embedded in layered media, in this work we develop a new theory in the spectral domain with proper mathematical tools that allow for the representation of scattering problems immersed in arbitrary linear media of an angular shape. In particular, these new formulations are in the spectral domain (Laplace domain) without introducing angular complex planes, and as such are not limited to *one-propagation-constant* problems. In [34], we developed the general theory in abstract form to model angular regions filled by arbitrary linear media and we reported its implementation only for isotropic media.

In the present work, we propose a complete theoretical package for solving diffraction problems with impenetrable wedges immersed in an arbitrary linear medium; in addition, this package is extendable to multiple penetrable angular regions. The proposed method exploits the combination and the extension of powerful mathematical tools developed in different contexts. The first tool is the Bresler–Marcuvitz (BM) transverse equation theory for layered media [33,35], the second is the characteristic Green function procedure [36,37], the third one is the Wiener–Hopf technique [33,38] in its generalized form [11,12], and the fourth one (which is a completely novel contribution) is the direct application of Fredholm factorization to generalized Wiener–Hopf equations (GWHEs).

The method starts with an extension of transverse equation theory for layered arbitrary linear media applied to the stratification of an angular shaped region with the help of abstract BM notation. We then apply the characteristic Green function procedure to obtain the solution of equations in angular geometries. The solutions defined at the faces of the angular region are spectral functional equations that relate continuous (tangential) field components of the two faces delimiting a homogeneous angular region. The application of boundary conditions yields a system of generalized Wiener–Hopf equations (GWHEs), where *generalized* means that the field components of each face are defined into different complex planes but related to one another. The GWHEs preserve the characteristic form of classical Wiener–Hopf equations (CWHEs), where the system of equations presents a kernel and plus and minus unknowns; however, the plus and minus unknowns are defined into different complex planes which are related to one another. The functional equations

and GWHEs of angular regions can be suitably interpreted with a network formalism, as is common for classical layered regions using transmission line theory. This circuit/network modeling representation of angular regions allows for the description of the technique with systematic steps to avoid redundancy. This capability is particularly useful when dealing with complex scattering problems, where we break down the complexity of a geometry into subdomains of canonical shape. These subdomains are modeled via spectral functional equations or related integral representations that can be interpreted through a network approach (obtained once and for all) and are capable of modeling the entire complex problem through the composition of circuital relationships; see, for instance, [30–32].

In the presence of an isotropic medium (and further special cases of more general media), a suitable mapping reduces the GWHEs to CWHEs, which in certain cases are amenable of exact solutions; alternatively, we can resort to the semi-analytical/approximate general-purpose factorization method, that is, Fredholm factorization, which reduces the factorization problem to Fredholm Integral Equations (FIEs) of the second kind. This technique was presented in the early 2000s for CWHEs; it was first effectively applied in impenetrable and penetrable wedge problems immersed in isotropic media [11,12], and more recently in isotropic complex scattering problems [30–32].

The main constraint in the present work resides in the complexity of media that do not allow mappings between complex planes of GWHEs for their transformation into CWHEs. Consequently, when dealing with arbitrary linear media in particular, we propose relying on a novel version of the versatile approximate method known as Fredholm factorization. Here, for the first time, we apply the Fredholm factorization method directly to GWHEs as a regularization tool. This regularized method can also be derived before the imposition of boundary conditions, i.e., directly on spectral functional equations (that is, before obtaining the GWHEs of the problem) by reversing the classical order of imposing boundary conditions and then applying Fredholm regularization to obtain the same effectiveness. We call this new methodology *direct Fredholm factorization*.

We observe that the impossibility of mapping GWHEs to CWHEs in arbitrary linear media is similar to the impossibility of defining a unique angular complex plane for the SM, KL, and WH methods; however, the new WH methodology proposed in this study overcomes this obstacle by resorting to direct Fredholm factorization applied to GWHEs.

From the solution of the GWHEs inherent to the angular region problem, we obtain the spectral representation of the field components along the faces delimiting homogeneous angular regions. The complete spectral analysis of the diffraction problems is then obtained by resorting again to spectral functional equations written for an arbitrary azimuthal direction. Finally, spectral inversion yields field components in the physical domain for any point in the angular regions. An alternative method for obtaining the field is also proposed; because of the linearity, it is based on the use of superposition on spectral representations prior to spectral inversion by identifying the spectral contributions of the faces of the angular regions through the equivalence theorem.

All of the theoretical properties of the mathematical statements are fully described in the text, although completely rigorous mathematical proofs are sometimes limited. On the other hand, validation of the proposed novel theoretical package through examples is reported, starting by demonstrating the effectiveness of direct Fredholm factorization applied to GWHEs in the scattering from a PEC wedge immersed in an isotropic medium and ending with validation of functional equations of angular regions in arbitrary linear media with the analysis of a PEC half-plane immersed in particular anisotropic media.

While implementing the method, we observe that the main difficulty resides in correctly estimating the kernel functions in the GWHEs and the corresponding FIE formulations for the presence of multivalued functions that need particular attention in their definition and calculation. The following sections highlight all multivalued functions and their correct estimations and assumptions.

In summary, we highlight in brief the main novelties of this work with respect to the state of the art reported in the introduction:

- Development of a novel spectral method capable of handling scattering in arbitrary linear media with multiple propagation constants.
- Introduction of a novel solution procedure for GWHEs, particularly for those with multiple propagation constants, which we call direct Fredholm factorization.
- A description of spectral functional equations and related integral representations for angular regions filled by arbitrary linear media in terms of the network interpretation.
- Computation of the field at each point within the angular region by resorting to the equivalence theorem and using Kirchhoff representations in the spectral domain;
- Improving the quality of the approximate spectral solutions by reimposing GWHEs, referred to as iteration.

It is important to highlight that the applicability of the proposed WH technique to arbitrary linear media resides in its formulation directly in the Laplace domain while avoiding other complex planes; notably, other techniques such as SM use complex angular planes based on Sommerfeld representations, which are applicable only to isotropic media or special cases of anisotropic media. Moreover, although SM also uses Fredholm integral equations in the complex angular plane for approximate solutions [2,6], it is limited to isotropic media; again, the proposed WH method is extended to arbitrary linear media with direct Fredholm factorization because it is directly formulated in the Laplace domain. Furthermore, another important result is that while Sommerfeld–Malyuzhinets solutions combined with asymptotic methods require analytical extension of the spectral solutions in the improper sheet to compute the far field, our application of equivalence theorem in the context of the proposed method can be directly applied to approximate WH spectral solutions in the Laplace domain. This result is due to the direct solution of the GWHEs which provides the complete spectra of the field on the two faces of an angular region, useful and sufficient for asymptotic estimations.

This article is organized into seven sections and one appendix. In Section 1, we introduce the motivation and the scope of the present work, then report the state of the art related to the spectral analysis of diffraction in complex media. Section 2 presents the main mathematical steps for obtaining spectral functional equations in an angular region filled by an arbitrary linear medium and with arbitrary boundary conditions, starting from the abstract BM notation for transverse equations in layered planar regions and extending this theory to layered angular regions filled by arbitrary linear media. Section 3 develops the theory, starting from the spectral functional equation to obtain regularized integral representations for angular regions in arbitrary linear media with the direct application of the Fredholm factorization method. If boundary conditions are applied, the representations are GWHEs. Section 4 presents the route for obtaining an asymptotic estimation of the far field inside the angular region after the face spectra on the two limiting faces have been obtained. To demonstrate the efficacy of the proposed methodology, in particular direct Fredholm factorization, Section 5 reports a validation using the simple case of a PEC wedge immersed in an isotropic medium. To further validate the method in arbitrary linear media, Section 6 presents an example of the application of functional equations in arbitrary linear media, specifically, a PEC half-plane immersed in a gyrotropic medium. Section 7 presents the conclusion of the paper. Finally, the Appendix A reports the full and explicit formulas and equations, as abstract notation is used in the main text with the dual purpose of enhancing readability and ensuring completeness.

2. Spectral Functional Equations in an Angular Region Filled by Arbitrary Linear Media

Spectral functional equations in angular regions filled by arbitrary linear media are obtained by exploiting the combination and extension of the following powerful mathematical tools developed in different contexts: first, the Bresler–Marcuvitz (BM) transverse equation theory for layered media [33,35], and second, the characteristic Green function procedure [36,37]. In this section, following [34], we first briefly revisit the BM theory for layered planar arbitrary linear media as a fundamental step in analyzing layered angular regions. We then apply the characteristic Green function procedure to derive solutions of

the obtained system of differential equations. Finally, we provide the spectral functional equations by evaluating the solution at the faces of the angular region. In particular, the functional equations relate continuous (tangential) spectral field components defined at the two faces of the angular region.

We start from the application of BM theory to Maxwell's equations in layered arbitrary nondispersive homogeneous linear media with tensorial constitutive relations (i.e., bianisotropic media [25–27]):

$$\begin{aligned} \boldsymbol{D} &= \underline{\underline{\varepsilon}} \cdot \boldsymbol{E} + \underline{\underline{\xi}} \cdot \boldsymbol{H} \\ \boldsymbol{B} &= \underline{\underline{\zeta}} \cdot \boldsymbol{E} + \underline{\underline{\mu}} \cdot \boldsymbol{H} \end{aligned} \tag{1}$$

where the electric and magnetic fields $(\boldsymbol{E}, \boldsymbol{H})$ are related to the electric and magnetic fluxes $(\boldsymbol{D}, \boldsymbol{B})$ and the tensors $(\underline{\underline{\varepsilon}}, \underline{\underline{\mu}}, \underline{\underline{\xi}}, \underline{\underline{\zeta}})$ are, respectively, the electric permittivity, the magnetic permeability, and the two magneto-electric coupling parameters.

By assuming

(a) Cartesian coordinates (z, x, y),
(b) $e^{+j\omega t}$ time–harmonic field dependence,
(c) Invariant geometry along z and stratification along y, and
(d) Sources constituted of plane waves with z-dependence $e^{-j\alpha_o z}$, where α_o depends on the skewness angle with respect to z (with $\alpha_o = 0$ at normal incidence on z),

We obtain the transverse differential equations in matrix form for layered planar media:

$$-\frac{\partial}{\partial y}\boldsymbol{\psi_y}(x,y) = \boldsymbol{M_y}(-j\alpha_o, \frac{\partial}{\partial x}) \cdot \boldsymbol{\psi_y}(x,y) \tag{2}$$

where $\boldsymbol{\psi_y}$ is the four-dimensional column vector (Throughout the article, we assume the notation $|\,|$ for vectors and not for the modulus of a vector).

$$\boldsymbol{\psi_y} = |\boldsymbol{E_t^t}, \boldsymbol{H_t^t}|^t, \;\; with \; \boldsymbol{E_t} = |E_z, E_x|^t, \; \boldsymbol{H_t} = |H_z, H_x|^t. \tag{3}$$

Based on the nature of Maxwell's equations, $\boldsymbol{M_y}(-j\alpha_o, \frac{\partial}{\partial x})$ is a second-order four-dimensional matrix differential operator of the form

$$\boldsymbol{M_y}(-j\alpha_o, \frac{\partial}{\partial x}) = \boldsymbol{M_{yo}} + \boldsymbol{M_{y1}}\frac{\partial}{\partial x} + \boldsymbol{M_{y2}}\frac{\partial^2}{\partial x^2}, \tag{4}$$

where the explicit forms of the matrices $\boldsymbol{M_{yo}}, \boldsymbol{M_{y1}}, \boldsymbol{M_{y2}}$ for an arbitrarily linear medium (1) are reported in Appendix A with (A2)–(A9). The application of the Fourier transform along x reduces (2) to

$$-\frac{d}{dy}\boldsymbol{\psi_y}(\eta,y) = \boldsymbol{M_y}(-j\alpha_o, -j\eta) \cdot \boldsymbol{\psi_y}(\eta,y), \tag{5}$$

where $\boldsymbol{\psi_y}(x,y) \doteq \frac{1}{2\pi}\int_{-\infty}^{\infty} \boldsymbol{\psi_y}(\eta,y)e^{-j\eta x}d\eta$ and

$$\boldsymbol{M_y}(-j\alpha_o, -j\eta) = \boldsymbol{M_{yo}} - j\eta\boldsymbol{M_{y1}} - \eta^2\boldsymbol{M_{y2}}. \tag{6}$$

We introduce here an analysis of the operator $\boldsymbol{M_y}(-j\alpha_o, -j\eta)$ of the layered planar arbitrarily linear media; this is necessary to obtain the solution of (2) in terms of eigenvalues, eigenvectors (with the characteristic Green function procedure), and boundary conditions. The same analysis is needed to obtain a solution for layered angular arbitrarily linear media. Supposing for the general case (removing exceptions) that $\boldsymbol{M_y}$ is semi-simple, we compute its eigenvalues λ_i and eigenvectors $\boldsymbol{u_i}$ as follows:

$$\boldsymbol{M_y u_i} = \lambda_i \boldsymbol{u_i} \tag{7}$$

i.e.,

$$\boldsymbol{M_y} = \boldsymbol{U_y J_y U_y^{-1}} \tag{8}$$

where $\boldsymbol{J_y} = diag\{\lambda_1, \lambda_2, \lambda_3, \lambda_4\}$ and $\boldsymbol{U_y} = (\boldsymbol{u_1}, \boldsymbol{u_2}, \boldsymbol{u_3}, \boldsymbol{u_4})$ (dependence on η and α_o is omitted). The computation of the eigenvalues is obtained from the zeros of the characteristic equation of order four (9), the coefficients of which can be written using Bocher's formula, as shown below [39].

$$det[\boldsymbol{M_y} - \lambda_i \boldsymbol{I}] = \lambda_i^4 + a\lambda_i^3 + b\lambda_i^2 + c\lambda_i + d = 0 \tag{9}$$

$$a = -tr(\boldsymbol{M_y}),\ b = -\frac{a\,tr(\boldsymbol{M_y}) + tr(\boldsymbol{M_y^2})}{2},\ c = -\frac{b\,tr(\boldsymbol{M_y}) + a\,tr(\boldsymbol{M_y^2}) + tr(\boldsymbol{M_y^3})}{3},\ d = det[\boldsymbol{M_y}] \tag{10}$$

This yields the following four eigenvalues:

$$\lambda_1 = -\frac{a}{4} + \frac{\sqrt{T} + \sqrt{M_a + Q}}{2},\ \lambda_2 = -\frac{a}{4} + \frac{\sqrt{T} - \sqrt{M_a + Q}}{2}, \tag{11}$$

$$\lambda_3 = -\frac{a}{4} - \frac{\sqrt{T} + \sqrt{M_a - Q}}{2},\ \lambda_4 = -\frac{a}{4} - \frac{\sqrt{T} - \sqrt{M_a - Q}}{2} \tag{12}$$

where

$$T = \frac{a^2}{4} + \frac{-3ac + b^2 + 12d}{3\sqrt[3]{u}} + \frac{\sqrt[3]{u} - 2b}{3},\ Q = -\frac{a^3 - 4ab + 8c}{4\sqrt{T}},\ M_a = \frac{3a^2}{4} - 2b - T \tag{13}$$

with

$$u = \frac{\sqrt{s} + v}{2},\ v = 9\left(3a^2d - abc - 8bd + 3c^2\right) + 2b^3,\ s = v^2 - 4\left(-3ac + b^2 + 12d\right)^3. \tag{14}$$

We note that the column vectors $\boldsymbol{u}_{i=1,2,3,4}$ of $\boldsymbol{U_y}$ provide a basis in the space $\mathbb{C}^4$, where we define the transverse electromagnetic field $\boldsymbol{\psi_y}$, while the column vectors $\boldsymbol{v}_{i=1,2,3,4}$ of

$$\boldsymbol{V_y} = \boldsymbol{U_y^{-1}} \tag{15}$$

in the reciprocal space will be fundamental in obtaining functional equations through the characteristic Green function procedure. Each couple $(\boldsymbol{u_i}, \boldsymbol{v_i})$ is related to a single λ_i for which the explicit forms are, in general, the cumbersome expressions reported in (11) and (12), which depend on η. In the most simple case, i.e., the isotropic medium ($\underline{\underline{\boldsymbol{\varepsilon}}} = \varepsilon \underline{\underline{\boldsymbol{I}}}$, $\underline{\underline{\boldsymbol{\mu}}} = \mu \underline{\underline{\boldsymbol{I}}}$, $\underline{\underline{\boldsymbol{\xi}}} = \underline{\underline{\boldsymbol{\zeta}}} = \underline{\underline{\boldsymbol{0}}}$), λ_i assumes the following forms:

$$\lambda_1 = \lambda_2 = -\lambda_3 = -\lambda_4 = \sqrt{(\alpha_o^2 + \eta^2) - k^2} = j\sqrt{(k^2 - \alpha_o^2) - \eta^2} = j\xi_{iso},\ k = \omega\sqrt{\varepsilon\mu} \tag{16}$$

where in the presence of losses ($k = k_r - jk_i$; $k_r, k_i > 0$) we have $\mathrm{Re}[\lambda_{1,2}] > 0$ and $\mathrm{Re}[\lambda_{3,4}] < 0$, which are respectively related to progressive ($i = 1, 2$) and regressive ($i = 3, 4$) waves with regard to y of form $e^{-j\eta x}e^{-\lambda_i y}e^{-j\alpha_o z}$. In this framework, we associate the direction of propagation with attenuation phenomena; we let the phase variation be free of constraints to allow modeling of left-handed materials. In a general arbitrary (even small) lossy linear medium, we always have two eigenvalues (say, $i = 1, 2$) with a positive real part $\lambda_i = +j\xi_i$ representing progressive waves and two (say, $i = 3, 4$) with a negative real part $\lambda_i = -j\xi_i$ representing regressive waves, yielding all four y-longitudinal propagation constants with $\mathrm{Im}[\xi_i] < 0$ (y-progressive/regressive waves $e^{\mp j\xi_i y}$, i.e., assuming time-harmonic dependence $e^{+j\omega t}$, we have x, y, z progressive waves $e^{-j\eta x}e^{-j\xi_i y}e^{-j\alpha_o z}$, respectively, with $\mathrm{Im}[\eta, \xi_i, \alpha_o] < 0$).

We affirm here the importance of retaining the generality of the medium; while investigating the scattering of objects immersed in arbitrary linear media, the scatterer can be

arbitrarily oriented with respect to the principal axis of the (crystal) medium. However, when the problem permits the definition of a coordinate system that coincides with the principal axes of the crystal medium, we obtain tensorial constitutive relations with diagonal tensors (1). These media are called biaxial, uniaxial, and isotropic, while the three terms in the diagonal are, respectively, all different, one different, and all equal. Other special cases are gyrotropic media, which represent media in which the tensorial constitutive relations are Hermitian with respect to the coordinate system and of the following type (in (17), we limit the description to the permittivity, i.e., a gyroelectric medium):

$$\underline{\underline{\boldsymbol{\varepsilon}}} = \begin{bmatrix} \varepsilon & +j\varepsilon_g & 0 \\ -j\varepsilon_g & \varepsilon & 0 \\ 0 & 0 & \varepsilon_a \end{bmatrix}. \tag{17}$$

Starting from planar layered regions, we extend the theory to angular-shaped regions of aperture γ filled by arbitrary linear media, as already done in Section 3 of [34] for angular regions filled by isotropic media. With reference to region 1 in Figure 1a, we derive from (2) the oblique transverse Equation (19) using an oblique system of Cartesian axes $(z, u \equiv x, v)$:

$$x = u + v\cos\gamma,\ y = v\sin\gamma, \tag{18}$$

$$-\frac{\partial}{\partial v}\boldsymbol{\psi_y}(u,v) = \boldsymbol{M}_\gamma(-j\alpha_o, \frac{\partial}{\partial u})\cdot\boldsymbol{\psi_y}(u,v). \tag{19}$$

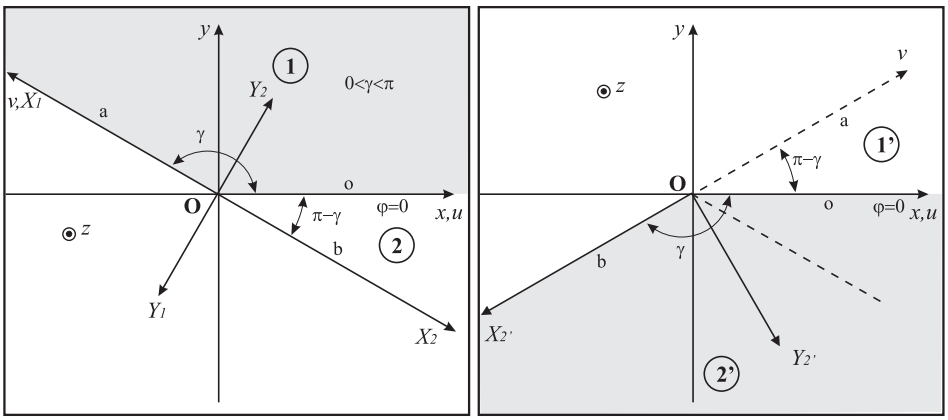

Figure 1. Angular regions and oblique Cartesian coordinates. (**a**) The figure reports the Cartesian coordinates z, x, y and the oblique Cartesian coordinate system $z, u \equiv x, v$ with reference to angular region 1 of aperture γ $(0 < \varphi < \gamma)$ with $0 < \gamma < \pi$, delimited by faces a and o. In the figure, a second region is identified $(-\pi + \gamma < \varphi < 0)$ delimited by faces b and o. The figure also reports the local-to-face Cartesian coordinate systems $Z_1 \equiv z, X_1, Y_1$ and $Z_2 \equiv z, X_2, Y_2$ for face a of region 1 and face b of region 2, respectively. The local-to-face Cartesian coordinate systems are obtained from the z, x, y Cartesian coordinate system through rotation for a positive γ and a negative $\pi - \gamma$, respectively. (**b**) The figure shows the new framework of the space divided into two angular regions, which is useful for the study of wedge structures. The figure reports both the Cartesian coordinates z, x, y and the oblique Cartesian coordinate system $z, u \equiv x, v$, where γ is the aperture angle of region $2'$. The figure also reports the local-to-face-b Cartesian coordinate system of region $2'$ $Z_{2'} \equiv z, X_{2'}, Y_{2'}$, which is obtained from the z, x, y Cartesian coordinate system through a rotation of an angle $-\gamma$. Finally, in both figures we also use cylindrical coordinates (z, ρ, φ).

The application of a Fourier transform along $u = x$ reduces (19) to

$$-\frac{d}{dv}\boldsymbol{\psi_y}(\eta,v) = \boldsymbol{M}_\gamma(-j\alpha_o, -j\eta)\cdot\boldsymbol{\psi_y}(\eta,v), \tag{20}$$

where $\boldsymbol{\psi_y}(u,v) \doteq \frac{1}{2\pi}\int_{-\infty}^{\infty} \boldsymbol{\psi_y}(\eta,v)e^{-j\eta u}d\eta$ and

$$\boldsymbol{M}_\gamma(-j\alpha_o,-j\eta) = \boldsymbol{M}_{\gamma o} - j\eta\boldsymbol{M}_{\gamma 1} - \eta^2\boldsymbol{M}_{\gamma 2}, \tag{21}$$

$$\boldsymbol{M_{\gamma o}} = \boldsymbol{M_{yo}}\sin\gamma, \quad \boldsymbol{M_{\gamma 1}} = \boldsymbol{M_{y1}}\sin\gamma - \boldsymbol{I_t}\cos\gamma, \quad \boldsymbol{M_{\gamma 2}} = \boldsymbol{M_{y2}}\sin\gamma. \tag{22}$$

Based on the link between $\boldsymbol{M}_\gamma$ and $\boldsymbol{M_y}$, we have $\boldsymbol{M}_\gamma$ with the same eigenvectors $\boldsymbol{u_i}$ of $\boldsymbol{M_y}$, and the following relationship between the eigenvalues $\lambda_{\gamma i}(\gamma)$ and λ_i can be obtained:

$$\lambda_{\gamma i}(\gamma) = j\eta\cos\gamma + \lambda_i\sin\gamma\ ,\ i = 1\cdots 4 \tag{23}$$

resulting in the following "oblique" v-longitudinal propagation constants:

$$m_i(\gamma) = -j\lambda_{\gamma i}(\gamma) = +\eta\cos\gamma + \xi_i\sin\gamma\ ,\ i = 1,2 \tag{24}$$

$$m_i(\gamma) = +j\lambda_{\gamma i}(\gamma) = -\eta\cos\gamma + \xi_i\sin\gamma\ ,\ i = 3,4 \tag{25}$$

which is in agreement with the relationship between λ_i and ξ_i as well as with the correlated progressive and regressive propagating interpretation along the longitudinal direction y and along the oblique "longitudinal" direction v (progressive/regressive $e^{\mp jm_iv}$). We note that the quantities $\boldsymbol{M}_\gamma(-j\alpha_o,-j\eta)$, $\lambda_{\gamma i}(\gamma)$, and $m_i(\gamma)$ depend on the geometrical parameter γ and on the spectral variable η.

With reference to region 1 in Figure 1a, we obtain the functional equations with a circuital interpretation as a mathematical manipulation of the solution of the differential Equation (19) using the Laplace domain $\tilde{\boldsymbol{\psi}}_{\boldsymbol{y}}(\eta,v) \doteq \int_0^{\infty} e^{j\eta\, u}\boldsymbol{\psi_y}(u,v)du$.

$$-\frac{d}{dv}\tilde{\boldsymbol{\psi}}_{\boldsymbol{y}}(\eta,v) = \boldsymbol{M}_\gamma(-j\alpha_o,-j\eta)\cdot\tilde{\boldsymbol{\psi}}_{\boldsymbol{y}}(\eta,v) + \boldsymbol{\psi_{sa}}(v),\ v>0 \tag{26}$$

$$\boldsymbol{\psi_{sa}}(v) = -\boldsymbol{M}_{\gamma 1}\cdot\boldsymbol{\psi_y}(0_+,v) + j\eta\ \boldsymbol{M}_{\gamma 2}\cdot\boldsymbol{\psi_y}(0_+,v) - \boldsymbol{M}_{\gamma 2}\cdot\frac{\partial}{\partial u}\boldsymbol{\psi_y}(u,v)\Big|_{u=0_+} \tag{27}$$

The benefit of using the Laplace transform is correlated with the incorporation of boundary conditions through initial conditions with the term $\boldsymbol{\psi_{sa}}(v)$. In (26)–(27), the condition $u = 0_+, v > 0$ imposes boundary conditions on the fields along face a in Figure 1a. The solution is obtained by using the characteristic Green function procedure [34] in terms of homogeneous and particular solutions, yielding the representation shown below.

$$\tilde{\boldsymbol{\psi}}_{\boldsymbol{y}}(\eta,v) = \sum_{i=1}^{4} C_i e^{-\lambda_{\gamma i}(\gamma)\,v}\boldsymbol{u_i} - \sum_{i=1}^{2}\boldsymbol{u_i}\boldsymbol{v_i}\cdot\int_0^{v} e^{-\lambda_{\gamma i}(\gamma)(v-v')}\boldsymbol{\psi_{sa}}(v')dv' + \sum_{i=3}^{4}\boldsymbol{u_i}\boldsymbol{v_i}\cdot\int_v^{\infty} e^{-\lambda_{\gamma i}(\gamma)(v-v')}\boldsymbol{\psi_{sa}}(v')dv' \tag{28}$$

Now, considering the asymptotic behavior in (28) of exponential functions in v for $v \to +\infty$, we need to have $C_3 = C_4 = 0$; at the same time, the first couple of integrals are null, as $Re[\lambda_{1,2}] > 0$ and $Re[\lambda_{3,4}] < 0$ are related to progressive and regressive waves, respectively. For this reason, setting $v = 0$, we obtain the following spectral field representation along face o:

$$\tilde{\boldsymbol{\psi}}_{\boldsymbol{o+}}(\eta) \doteq \tilde{\boldsymbol{\psi}}_{\boldsymbol{y}}(\eta,0) = C_1\boldsymbol{u_1} + C_2\boldsymbol{u_2} + \sum_{i=3}^{4}\boldsymbol{u_i}\boldsymbol{v_i}\cdot\int_0^{\infty} e^{-\lambda_{\gamma i}(\gamma)(v-v')}\boldsymbol{\psi_{sa}}(v')dv'. \tag{29}$$

By weighting (29) with the reciprocal vectors $\boldsymbol{v_3}, \boldsymbol{v_4}$ of $\boldsymbol{M}_\gamma$, we obtain the following functional equations:

$$\boldsymbol{v_i}\cdot\tilde{\boldsymbol{\psi}}_{\boldsymbol{o+}}(\eta) = \boldsymbol{v_i}\cdot\tilde{\boldsymbol{\psi}}_{\boldsymbol{sa+}}(-m_i(\gamma)), \quad i = 3,4 \tag{30}$$

where we use the following definition of the Laplace transform:

$$\tilde{\boldsymbol{\psi}}_{\boldsymbol{sa}+}(-m_i(\gamma)) \doteq \int_0^\infty e^{-jm_i(\gamma)v}\boldsymbol{\psi}_{\boldsymbol{sa}}(v)dv = \int_0^\infty e^{-jm_i(\gamma)\rho}\boldsymbol{\psi}_{\boldsymbol{sa}}(\rho)d\rho. \tag{31}$$

With reference to Figure 1a and its caption, analyzing and expanding $\tilde{\boldsymbol{\psi}}_{\boldsymbol{sa}+}(-m_i(\gamma))$ in (30) using Maxwell's equations, we rephrase the functional equations for region 1 as

$$\boldsymbol{v_i}\cdot\tilde{\boldsymbol{\psi}}_{\boldsymbol{o}+}(\eta) = \boldsymbol{v_i}\cdot\boldsymbol{T}(\gamma)\cdot\tilde{\boldsymbol{\psi}}_{\boldsymbol{a}+}(-m_i(\gamma),\gamma), \quad i=3,4, \tag{32}$$

where $\tilde{\boldsymbol{\psi}}_{\boldsymbol{o}+}(\eta)$ is the η Laplace transform of the tangent-to-face-o field components (i.e., at $\varphi=0$) in Cartesian (z,x,y) and cylindrical coordinates (z,ρ,φ) (omitting the z coordinate for invariance)

$$\begin{aligned}\tilde{\boldsymbol{\psi}}_{\boldsymbol{o}+}(\eta) = &\int_0^\infty |E_z(x,0),E_x(x,0),H_z(x,0),H_x(x,0)|^t e^{j\eta x}dx\\ &= \int_0^\infty |E_z(\rho,0),E_\rho(\rho,0),H_z(\rho,0),H_\rho(\rho,0)|^t e^{j\eta\rho}d\rho,\end{aligned} \tag{33}$$

where $\tilde{\boldsymbol{\psi}}_{\boldsymbol{a}+}(-m_i(\gamma),\gamma)$ is the $-m_i(\gamma)$ Laplace transform of the tangent-to-face-a field components (i.e., at $\varphi=\gamma$) in local-to-face-a Cartesian (z,X_1,Y_1) coordinates and global cylindrical coordinates (z,ρ,φ) (located at $\varphi=+\gamma$)

$$\begin{aligned}\tilde{\boldsymbol{\psi}}_{\boldsymbol{a}+}(-m_i(\gamma),\gamma) = &\int_0^\infty |E_z(X_1,0),E_{X_1}(X_1,0),H_z(X_1,0),H_{X_1}(X_1,0)|^t e^{-jm_i(\gamma)X_1}dx\\ &= \int_0^\infty |E_z(\rho,\gamma),E_\rho(\rho,\gamma),H_z(\rho,\gamma),H_\rho(\rho,\gamma)|^t e^{-jm_i(\gamma)\rho}d\rho,\end{aligned} \tag{34}$$

and

$$\boldsymbol{T}(\gamma) = \begin{pmatrix} \frac{\sin(\gamma)(\alpha_o\xi_{yy}+\zeta_{xy}\xi_{yy}\omega-\mu_{xy}\omega\epsilon_{yy})}{\omega(\mu_{yy}\epsilon_{yy}-\zeta_{yy}\xi_{yy})}+\cos(\gamma) & 0 & \frac{\sin(\gamma)(\alpha_o\mu_{yy}+\zeta_{xy}\mu_{yy}\omega-\zeta_{yy}\mu_{xy}\omega)}{\omega(\mu_{yy}\epsilon_{yy}-\zeta_{yy}\xi_{yy})} & 0\\ \frac{\sin(\gamma)(-\zeta_{zy}\xi_{yy}\omega+\eta\xi_{yy}+\mu_{zy}\omega\epsilon_{yy})}{\omega(\mu_{yy}\epsilon_{yy}-\zeta_{yy}\xi_{yy})} & 1 & \frac{\sin(\gamma)(\zeta_{yy}\mu_{zy}\omega-\zeta_{zy}\mu_{yy}\omega+\eta\mu_{yy})}{\omega(\mu_{yy}\epsilon_{yy}-\zeta_{yy}\xi_{yy})} & 0\\ \frac{\sin(\gamma)(-\alpha_o\epsilon_{yy}-\zeta_{yy}\omega\epsilon_{xy}+\xi_{xy}\omega\epsilon_{yy})}{\omega(\mu_{yy}\epsilon_{yy}-\zeta_{yy}\xi_{yy})} & 0 & \cos(\gamma)-\frac{\sin(\gamma)(\alpha_o\zeta_{yy}-\zeta_{yy}\xi_{xy}\omega+\mu_{yy}\omega\epsilon_{xy})}{\omega(\mu_{yy}\epsilon_{yy}-\zeta_{yy}\xi_{yy})} & 0\\ \frac{\sin(\gamma)(\xi_{yy}\omega\epsilon_{zy}-\epsilon_{yy}(\eta+\xi_{zy}\omega))}{\omega(\mu_{yy}\epsilon_{yy}-\zeta_{yy}\xi_{yy})} & 0 & \frac{\sin(\gamma)(\mu_{yy}\omega\epsilon_{zy}-\zeta_{yy}(\eta+\xi_{zy}\omega))}{\omega(\mu_{yy}\epsilon yy-\zeta_{yy}\xi_{yy})} & 1 \end{pmatrix} \tag{35}$$

Note that (32) are functional equations that relate the Laplace transforms of combinations of field components on the boundaries of angular region 1 in Figure 1a, i.e., face o $u>0$, $v=0$ ($\varphi=0$) and face a $u=0$, $v>0$ ($\varphi=\gamma$). Furthermore, we observe that the angle γ is essential in determining the impact of anisotropies through $\boldsymbol{T}(\gamma)$.

Repeating the same procedure for region 2 in Figure 1a, we obtain the functional equations as the solution of the differential Equation (19) in the Laplace domain using the left Laplace transform $\tilde{\boldsymbol{\psi}}_{\boldsymbol{y}}(\eta,v) \doteq \int_{-\infty}^0 e^{j\eta u}\boldsymbol{\psi}_{\boldsymbol{y}}(u,v)du$:

$$-\frac{d}{dv}\tilde{\boldsymbol{\psi}}_{\boldsymbol{y}}(\eta,v) = \boldsymbol{M}_\gamma(-j\alpha_o,-j\eta)\cdot\tilde{\boldsymbol{\psi}}_{\boldsymbol{y}}(\eta,v)+\boldsymbol{\psi}_{\boldsymbol{sb}}(v),\ v<0 \tag{36}$$

where $\boldsymbol{\psi}_{\boldsymbol{sb}}(v)$ has the same expression of $\boldsymbol{\psi}_{\boldsymbol{sa}}(v)$ (27) but with a different support $v<0$, and allows the incorporation of boundary conditions along face b ($u=0_+, v<0$). The application of the characteristic Green function procedure yields expression (28) for region 2 in Figure 1a, which is identical to that for region 1 except for C_i and the source term $\boldsymbol{\psi}_{\boldsymbol{sb}}(v)$, which depend on the local constitutive parameters and boundary conditions of region 2. Now, considering the asymptotic behavior of the exponential function in v for

$v \to -\infty$, we need to have $C_1 = C_2 = 0$; at the same time, the second couple of integrals are null. For this reason, setting $v = 0$, we obtain

$$\tilde{\boldsymbol{\psi}}_{o+}(\eta) \doteq \tilde{\boldsymbol{\psi}}_{\boldsymbol{y}}(\eta, 0) = C_3\boldsymbol{u_3} + C_4\boldsymbol{u_4} - \sum_{i=1}^{2} \boldsymbol{u_i v_i} \cdot \int_0^{\infty} e^{-\lambda_i(\gamma)(v-v')} \boldsymbol{\psi_{sb}}(v')dv'. \tag{37}$$

By weighting (37) with the reciprocal vectors $\boldsymbol{v_1}, \boldsymbol{v_2}$ of $\boldsymbol{M}_\gamma$, we obtain the functional equations

$$\boldsymbol{v_i} \cdot \tilde{\boldsymbol{\psi}}_{o+}(\eta) = -\boldsymbol{v_i} \cdot \tilde{\boldsymbol{\psi}}_{sb+}(-m_i(\gamma)), \quad i = 1, 2, \tag{38}$$

where we have used the definition of the v left Laplace transform

$$\tilde{\boldsymbol{\psi}}_{sb+}(-m_i(\gamma)) \doteq \int_{-\infty}^{0} e^{-jm_i(\gamma)v} \boldsymbol{\psi_{sb}}(v)dv = \int_0^{\infty} e^{-jm_i(\gamma)\rho} \boldsymbol{\psi_{sb}}(-\rho)d\rho. \tag{39}$$

Note the differences and similarities between Laplace transformations (31) and (39), which yield the same definition of the $-m_i(\gamma)$ Laplace transform in ρ but are applied to different quantities. Furthermore, the regularity properties of the $-m_i(\gamma)$ Laplace transform are inherited from ξ_i ($Im[\xi_i] < 0$) according to (24)–(25).

With reference to Figure 1a and its caption, analyzing and expanding $\tilde{\boldsymbol{\psi}}_{sb+}(-m_i(\gamma))$ in (38), we rephrase the functional equations into

$$\boldsymbol{v_i} \cdot \tilde{\boldsymbol{\psi}}_{o+}(\eta) = -\boldsymbol{v_i} \cdot \boldsymbol{T}(\gamma) \cdot \boldsymbol{P} \cdot \tilde{\boldsymbol{\psi}}_{b+}(-m_i(\gamma), -\pi + \gamma), \quad i = 1, 2. \tag{40}$$

In (40), $\boldsymbol{T}(\gamma)$ is again (35); as for region 1, $\boldsymbol{P} = diag\{1, -1, 1, -1\}$ is needed for $v = -X_2$ in region 2 with respect to $v = X_1$ in region 1, $\tilde{\boldsymbol{\psi}}_{o+}(\eta)$ is the η Laplace transform of the tangent-to-face-o field components reported in (33), and $\tilde{\boldsymbol{\psi}}_{b+}(-m_i(\gamma), -\pi + \gamma)$ is the $-m_i(\gamma)$ Laplace transform of the tangent-to-face-b field components (i.e., at $\varphi = -\pi + \gamma$) in the local-to-face-b Cartesian (z, X_2, Y_2) coordinates and global cylindrical coordinates (z, ρ, φ) of Figure 1a.

$$\begin{aligned} \tilde{\boldsymbol{\psi}}_{b+}(-m_i(\gamma), -\pi + \gamma) &= \int_0^{\infty} |E_z(X_2, 0), E_{X_2}(X_2, 0), H_z(X_2, 0), H_{X_2}(X_2, 0)|^t e^{-jm_i(\gamma)X_2} dx \\ &= \int_0^{\infty} |E_z(\rho, -\pi + \gamma), E_\rho(\rho, -\pi + \gamma), H_z(\rho, -\pi + \gamma), H_\rho(\rho, -\pi + \gamma)|^t e^{-jm_i(\gamma)\rho} d\rho \end{aligned} \tag{41}$$

While considering the wedge scattering problem with symmetry with respect to the x axis, in combination with region 1 in Figure 1a, we need to consider region 2′ in Figure 1b, where $\gamma \to \pi - \gamma$ with respect to region 2 in Figure 1a, i.e., for the same face a, we change the orientation of face b at $\varphi = \gamma$ from $\varphi = -\pi + \gamma$ to $\varphi = -\gamma$. The functional equations of region 2′ become

$$\boldsymbol{v_i} \cdot \tilde{\boldsymbol{\psi}}_{o+}(\eta) = -\boldsymbol{v_i} \cdot \boldsymbol{T}(\pi - \gamma) \cdot \boldsymbol{P} \cdot \tilde{\boldsymbol{\psi}}_{b+}(-m_i(\pi - \gamma), -\gamma), \quad i = 1, 2, \tag{42}$$

where

$$\begin{aligned} \tilde{\boldsymbol{\psi}}_{b+}(-m_i(\pi - \gamma), -\gamma) &= \int_0^{\infty} |E_z(X_2, 0), E_{X_2}(X_2, 0), H_z(X_2, 0), H_{X_2}(X_2, 0)|^t e^{-jm_i(\pi-\gamma)X_2} dx \\ &= \int_0^{\infty} |E_z(\rho, -\gamma), E_\rho(\rho, -\gamma), H_z(\rho, -\gamma), H_\rho(\rho, -\gamma)|^t e^{-jm_i(\pi-\gamma)\rho} d\rho, \end{aligned} \tag{43}$$

which is the $-m_i(\pi - \gamma)$ Laplace transform of the tangent-to-face-b field components (i.e., now at $\varphi = -\gamma$) in local-to-face-b Cartesian (z, X_2, Y_2) coordinates and global cylindrical coordinates (z, ρ, φ) in Figure 1b. Note that in (42) we assumed that region 2′ is homogeneous to region 1, yielding the same u_i, v_i; otherwise, specific vectors would be needed. Equations (42) are functional equations that relate the Laplace transforms of combinations

of field components on the boundaries of the angular region $2'$ in Figure 1b, i.e., face o $u > 0$, $v = 0$ ($\varphi = 0$) and face b $u = 0$, $v < 0$ ($\varphi = -\gamma$). In (42), note the new dependence of $\boldsymbol{T}(\cdot)$ (35) on $\pi - \gamma$ due to the effect of anisotropies while changing the orientation of face b from $-\pi + \gamma$ to $-\gamma$. Furthermore, in the case of symmetric media ($\lambda_{1,2} = -\lambda_{3,4}$), we have $m_{3,4}(\gamma) = m_{1,2}(\pi - \gamma)$; see (24)–(25).

In general, the system of functional equations in (32) and (42) allows for the analysis of angular regions that are symmetric with respect to the x axis; these are at the base of the analysis of scattering problems constituted by impenetrable and penetrable wedges surrounded/made by arbitrary linear media. In the following, to investigate a practical scattering problem, we impose boundary conditions at the faces of each angular region on the functional Equations (32) and (42), yielding a system of GWHEs.

3. From Functional Equations to GWHEs and Their Regularized Integral Representations with a Network Interpretation

Network representations of angular regions in isotropic media for electromagnetic scattering were extensively studied in multiple spectral domains in [13] using algebraic and integral formalisms. The proposed equations were effectively applied in several works to practical wedge scattering problems; see [11,12] and the references therein. Furthermore, network formalisms have been effectively applied for complex canonical problems containing angular and layered regions in isotropic media; see for instance the double wedge [31], flanged dielectric loaded waveguide [32], and wedge over dielectric layer [30], among others.

In arbitrary linear media, the system of functional Equations (32) and (42),

$$\begin{aligned} &\boldsymbol{v_i} \cdot \tilde{\boldsymbol{\psi}}_{o+}(\eta) = \boldsymbol{v_i} \cdot \boldsymbol{T}(\gamma) \cdot \tilde{\boldsymbol{\psi}}_{a+}(-m_i(\gamma), \gamma), \quad i = 3,4 \\ &\boldsymbol{v_i} \cdot \tilde{\boldsymbol{\psi}}_{o+}(\eta) = -\boldsymbol{v_i} \cdot \boldsymbol{T}(\pi - \gamma) \cdot \boldsymbol{P} \cdot \tilde{\boldsymbol{\psi}}_{b+}(-m_i(\pi - \gamma), -\gamma), \quad i = 1,2 \end{aligned} \tag{44}$$

constitutes two systems of network relations that link the spectral field components in region 1 and region $2'$ (Figure 1), respectively, via a sort of two-port transmission relations in algebraic form. Looking at the first system in (44), we have two combinations of $\tilde{\boldsymbol{\psi}}_{o+}(\eta)$ components (33) related to two combinations of $\tilde{\boldsymbol{\psi}}_{a+}(-m_i(\gamma), \gamma)$ components (34), i.e., with reference to Figure 1a, the tangential field components of face o are related to tangential field components of face a. A similar interpretation can be repeated for the second system in (44) for region 2 with field components defined at faces o and b, respectively, in $\tilde{\boldsymbol{\psi}}_{o+}(\eta)$ (33) and $\tilde{\boldsymbol{\psi}}_{b+}(-m_i(\pi - \gamma), -\gamma)$ (43).

We further note that in (44) the components of face o and face a, b are functions of the spectral variables η and $-m_i(\cdot)$, respectively, which are related to one another via (24)–(25). We can reverse the role of the variables η and $-m_i(\cdot)$ in the arguments of the components of these faces. In this way, we double the equations of region 1, i.e., the first line of (44), which is again reported in (45), yielding the second line of (45), which relates the components of face a (now functions of the variable η) to the components of face o (now functions of $-m_i(\cdot)$). The second line of (45) is obtained by defining region 1 as region $2'$ (Figure 1) after a clockwise rotation of an angle $+\gamma$, yielding the following complete set of equations for region 1:

$$\begin{aligned} &\boldsymbol{v_i} \cdot \tilde{\boldsymbol{\psi}}_{o+}(\eta) = \boldsymbol{v_i} \cdot \boldsymbol{T}(\gamma) \cdot \tilde{\boldsymbol{\psi}}_{a+}(-m_i(\gamma), \gamma), \quad i = 3,4, \\ &\boldsymbol{v}_{iY_1} \cdot \tilde{\boldsymbol{\psi}}_{a+}(\eta) = -\boldsymbol{v}_{iY_1} \cdot \boldsymbol{T}_{Y_1}(\pi - \gamma) \cdot \boldsymbol{P} \cdot \tilde{\boldsymbol{\psi}}_{o+}(-m_{iY_1}(\pi - \gamma), -\gamma), \quad i = 1,2. \end{aligned} \tag{45}$$

In the second pair of Equation (45), we have used the subscript Y_1 to refer to a rotated coordinated system (z, X_1, Y_1) with respect to (z, x, y); see region 1 in Figure 2a and the related region $2'$ in Figure 2b.

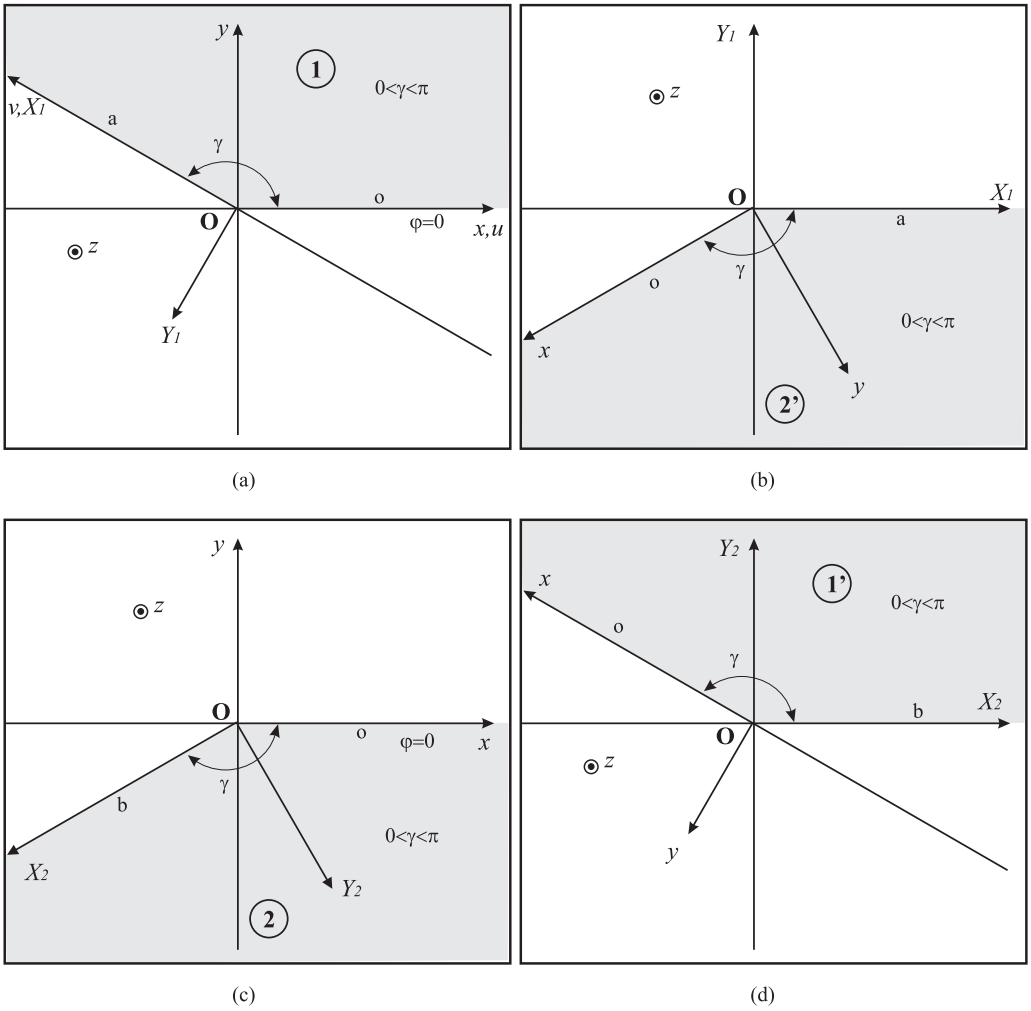

Figure 2. (**a**) Angular region 1 of aperture γ, which is delimited by faces a and o with the original reference Cartesian coordinate system z, x, y. The figure also reports the local-to-face-a Cartesian coordinate systems $Z_1 \equiv z, X_1, Y_1$. (**b**) Angular region 1 after a clockwise rotation of an angle γ, becoming region $2'$. The figure shows the reference systems of region 1 after the rotation. (**c**) Angular region 2 of aperture γ, which is delimited by faces b and o with the original reference Cartesian coordinate system z, x, y. The figure also reports the local-to-face-b Cartesian coordinate systems $Z_2 \equiv z, X_2, Y_2$. (**d**) Angular region 2 after a clockwise rotation of an angle γ, becoming region $1'$. The figure shows the reference systems of region 2 after the rotation.

We note that the second pair of equations in (45) can be easily derived by studying the classical region $2'$ (see the second pair of equations in (44)) except with modified definitions of the quantities $\boldsymbol{v}_{i\boldsymbol{Y}_1}, \boldsymbol{T}_{\boldsymbol{Y}_1}(\gamma)$, $m_{iY_1}(\gamma)$ (from $\lambda_{iY_1}(\gamma)$) because of their dependence on the constitutive tensorial parameters $(\underline{\underline{\boldsymbol{\varepsilon}}}, \underline{\underline{\boldsymbol{\mu}}}, \underline{\underline{\boldsymbol{\xi}}}, \underline{\underline{\boldsymbol{\zeta}}})$ of region 1, which are redefined in the reference coordinate system (z, X_1, Y_1), i.e., $(\underline{\underline{\boldsymbol{\varepsilon}}}_{Y_1}, \underline{\underline{\boldsymbol{\mu}}}_{Y_1}, \underline{\underline{\boldsymbol{\xi}}}_{Y_1}, \underline{\underline{\boldsymbol{\zeta}}}_{Y_1})$, for example,

$$\underline{\underline{\boldsymbol{\varepsilon}}}_{Y_1} = \underline{\underline{\boldsymbol{R}}}_{Y_1}^{-1} \cdot \underline{\underline{\boldsymbol{\varepsilon}}} \cdot \underline{\underline{\boldsymbol{R}}}_{Y_1}, \quad \underline{\underline{\boldsymbol{R}}}_{Y_1} = \begin{pmatrix} \cos(\gamma) & -\sin(\gamma) & 0 \\ \sin(\gamma) & \cos(\gamma) & 0 \\ 0 & 0 & 1 \end{pmatrix}, \tag{46}$$

due to the rotation of $+\gamma$.

The same rationale is applied to region 2 to double the equations of that region (second line of (44), as also reported in (47)) by obtaining

$$\begin{aligned} \boldsymbol{v_{iY_2}} \cdot \tilde{\boldsymbol{\psi}}_{\boldsymbol{b}+}(\eta) &= \boldsymbol{v_{iY_2}} \cdot \boldsymbol{T_{Y_2}}(\gamma) \cdot \tilde{\boldsymbol{\psi}}_{\boldsymbol{o}+}(-m_{iY_2}(\gamma), \gamma), \quad i = 3, 4, \\ \boldsymbol{v_i} \cdot \tilde{\boldsymbol{\psi}}_{\boldsymbol{o}+}(\eta) &= -\boldsymbol{v_i} \cdot \boldsymbol{T}(\pi - \gamma) \cdot \boldsymbol{P} \cdot \tilde{\boldsymbol{\psi}}_{\boldsymbol{b}+}(-m_i(\pi - \gamma), -\gamma), \quad i = 1, 2. \end{aligned} \tag{47}$$

In the first pair of equations in (47), we have used the subscript Y_2 to make reference to a rotated coordinated system (z, X_2, Y_2) with respect to (z, x, y); see region 2 in Figure 2c and the related region $1'$ in Figure 2d. We note that the first pair of equations in (47) can be easily derived by studying the classical region 1 (see the first pair of equations in (44)) except with modified definitions of $\boldsymbol{v_{iY_2}}$, $\boldsymbol{T_{Y_2}}(\gamma)$, and $m_{iY_2}(\gamma)$ because of their dependence on the constitutive parameters $(\underline{\underline{\varepsilon}}, \underline{\underline{\mu}}, \underline{\underline{\xi}}, \underline{\underline{\zeta}})$, which are redefined in the reference coordinate system (z, X_2, Y_2), i.e., $(\underline{\underline{\varepsilon}}_{Y_2}, \underline{\underline{\mu}}_{Y_2}, \underline{\underline{\xi}}_{Y_2}, \underline{\underline{\zeta}}_{Y_2})$, for example,

$$\underline{\underline{\varepsilon}}_{Y_2} = \underline{\underline{R}}_{Y_2}^{-1} \cdot \underline{\underline{\varepsilon}} \cdot \underline{\underline{R}}_{Y_2}, \quad \underline{\underline{R}}_{Y_2} = \begin{pmatrix} \cos(\gamma) & \sin(\gamma) & 0 \\ -\sin(\gamma) & \cos(\gamma) & 0 \\ 0 & 0 & 1 \end{pmatrix}, \tag{48}$$

due to the rotation of $-\gamma$.

The sets of Equations (45) and (47) constitute a complete set of functional equations that respectively describe regions 1 and 2 in Figure 3. In the case of symmetric media (i.e., $\lambda_{1,2} = -\lambda_{3,4}$) we have $m_{3,4}(\gamma) = m_{1,2}(\pi - \gamma)$; see (24)–(25).

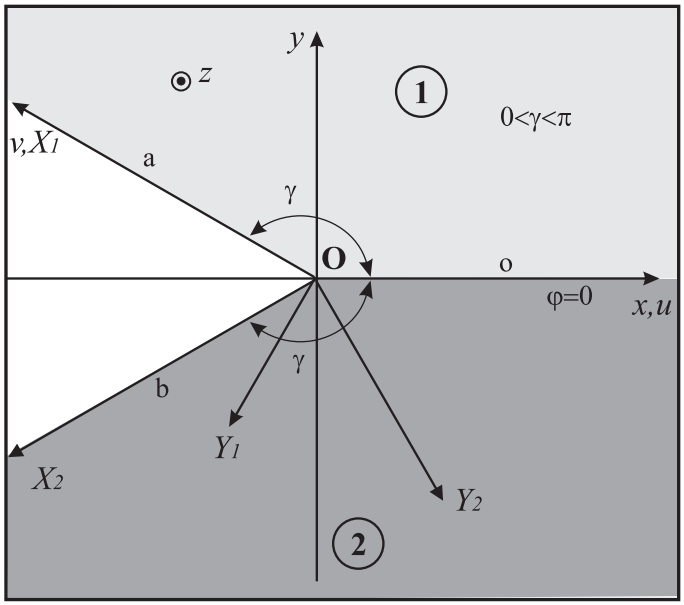

Figure 3. Two angular regions that are symmetric with respect to the x axis of the aperture angle γ and represent wedge problems immersed in arbitrary linear media; they are modeled using the complete sets of Equations in (45) and (47).

In isotropic media, it is always possible to introduce the angular complex plane w and the KL transform method [13], where functional equations become two-port admittance relations of the Norton type in integral and algebraic forms in a unique complex plane. In arbitrary linear media, the definition of such complex planes is not possible; however, a novel method that resorts to the following Cauchy decomposition formula in the $-m(\eta)$ plane is introduced. This is a fundamental tool that allows for the description of angular region problems in arbitrary linear media without introducing further complex planes other than the initial Laplace transforms. In particular, to obtain regularized integral equations from GWHEs, it is not necessary to map the GWHEs into CWHEs with suitable

transformations before the application of Fredholm factorization (originally ideated and valid only for the CWHEs). This revisited novel version of the regularization procedure can be called the *direct Fredholm factorization method* .

At the origin of this method, we introduce the following generalized form of the standard Cauchy decomposition formula in the $-m(\eta)$ plane (i.e., one of the $m_i(\cdot)$ that all depends on η) applied to an arbitrary $F_+(-m(\eta))$ (i.e., the standard form is obtained simply by replacing $-m(\eta)$ with η):

$$F_+(-m(\eta)) = \frac{1}{2\pi j}\int_{-\infty}^{\infty}\frac{F_+(\eta')}{\eta'+m(\eta)}d\eta' + F_+^{n.s.}(-m(\eta)),\ \eta\in\mathbb{R} \tag{49}$$

where $F_+^{n.s.}(-m(\eta))$ is the non-standard contribution of $F_+(-m(\eta))$ in the $-m(\eta)$ plane. Assuming a lossy medium, we observe that, in general, $-m(\eta)$ is located with the positive imaginary part for $\eta\in\mathbb{R}$, i.e., it is in the upper half-plane of complex plane η; thus, the application of (49) to plus functions is justified. For example, see Figure 4, where we have assumed that $k = 1-0.1j$ and $\gamma = 0.7\pi$, yielding a path of $-m(t)$ for $t\in\mathbb{R}$ from right to left because of $\gamma > \pi/2$. On the contrary, for $\gamma < \pi/2$ we obtain a similar path located in the upper half-plane, but in the opposite direction. We anticipate that the application of (49) to GWHEs with multiple propagation constants, i.e., with more than one $m_i(\eta)$, is fundamental for developing a solution in the η plane, as (49) transforms the GWHEs into integral equations in the unique complex plane η.

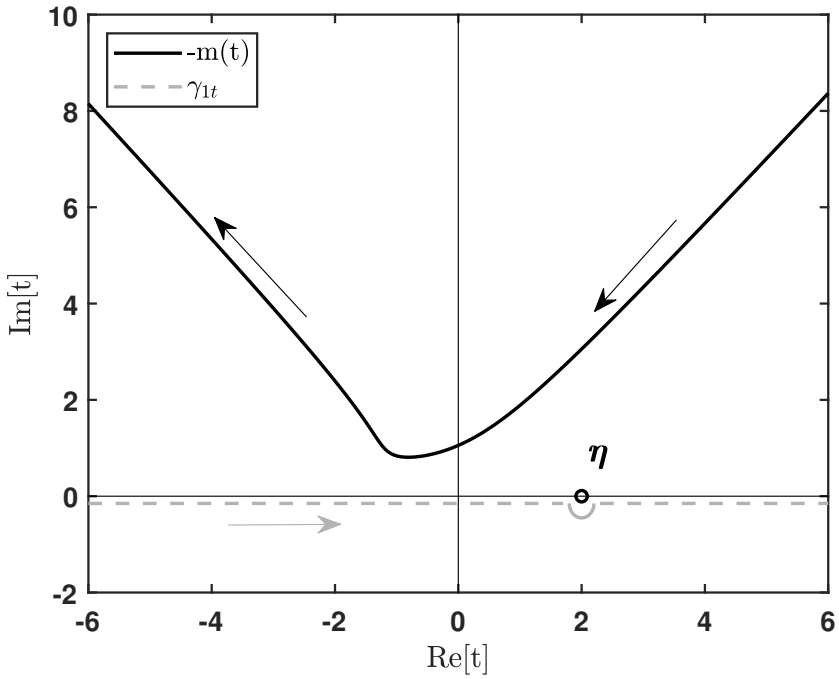

Figure 4. Cauchy *smile* contour integration line γ_{1t} and an example of line $-m(t)$ for $t\in\mathbb{R}$, $k = 1-0.1j$, $\gamma = 0.7\pi$ (if $\gamma < \pi/2$, then the behavior of $-m(t)$ has a similar path but opposite direction; to intuitively understand this property in an isotropic medium, consider the definition of m in the w plane for supplementary angles γ).

The complete sets of Equation (45) for region 1 can be represented in the following form:

$$\begin{aligned}
&A_{11}^E(\eta)E_{oz}(\eta) + A_{12}^E(\eta)E_{o\rho}(\eta) + A_{11}(\eta)H_{oz}(\eta) + A_{12}(\eta)H_{o\rho}(\eta) = B_{11}^E(\eta)E_{az}(-m_3) + B_{12}^E(\eta)E_{a\rho}(-m_3) + B_{11}(\eta)H_{az}(-m_3) + B_{12}(\eta)H_{a\rho}(-m_3)\\
&A_{21}^E(\eta)E_{oz}(\eta) + A_{22}^E(\eta)E_{o\rho}(\eta) + A_{21}(\eta)H_{oz}(\eta) + A_{22}(\eta)H_{o\rho}(\eta) = B_{21}^E(\eta)E_{az}(-m_4) + B_{22}^E(\eta)E_{a\rho}(-m_4) + B_{21}(\eta)H_{az}(-m_4) + B_{22}(\eta)H_{a\rho}(-m_4)\\
&A_{31}^E(\eta)E_{az}(\eta) + A_{32}^E(\eta)E_{a\rho}(\eta) + A_{31}(\eta)H_{az}(\eta) + A_{32}(\eta)H_{a\rho}(\eta) = B_{31}^E(\eta)E_{oz}(-m_1) + B_{32}^E(\eta)E_{o\rho}(-m_1) + B_{31}(\eta)H_{oz}(-m_1) + B_{32}(\eta)H_{o\rho}(-m_1)\\
&A_{41}^E(\eta)E_{az}(\eta) + A_{42}^E(\eta)E_{a\rho}(\eta) + A_{41}(\eta)H_{az}(\eta) + A_{42}(\eta)H_{a\rho}(\eta) = B_{41}^E(\eta)E_{oz}(-m_2) + B_{42}^E(\eta)E_{o\rho}(-m_2) + B_{41}(\eta)H_{oz}(-m_2) + B_{42}(\eta)H_{o\rho}(-m_2)
\end{aligned} \tag{50}$$

where the spectral field components of face o and face a are related to one another (Throughout this study, in spectral equations we assume a notation with two subscripts for the spectral field; the first subscript is related to the considered face (o, a, b) and the second to the field component (z, x, y)). Moreover, the complete set of equations for region 2 (47) has a similar representation. The imposition of boundary conditions makes these equations a well-posed mathematical problem, resulting in a system of GWHEs. In particular, if the region is surrounded by something modeled with impenetrable impedance boundary conditions, then we establish relations among field components on the boundary faces. On the contrary, if the region is surrounded by penetrable regions, then we establish continuity through tangent components to neighboring regions that provide further functional equations (coupled together). In any case, the types of completed functional equations and constraints with boundary conditions are always of the same form and are a well-posed mathematical problem of GWHEs.

As a simple example to illustrate the procedure, let us consider a problem constituted by only region 1 with PEC boundary conditions when filled by arbitrary linear media. In this case, we obtain

$$\begin{aligned}
A_{11}(\eta)H_{oz}(\eta) + A_{12}(\eta)H_{o\rho}(\eta) &= B_{11}(\eta)H_{az}(-m_3) + B_{12}(\eta)H_{a\rho}(-m_3)\\
A_{21}(\eta)H_{oz}(\eta) + A_{22}(\eta)H_{o\rho}(\eta) &= B_{21}(\eta)H_{az}(-m_4) + B_{22}(\eta)H_{a\rho}(-m_4)\\
A_{31}(\eta)H_{az}(\eta) + A_{32}(\eta)H_{a\rho}(\eta) &= B_{31}(\eta)H_{oz}(-m_1) + B_{32}(\eta)H_{o\rho}(-m_1)\\
A_{41}(\eta)H_{az}(\eta) + A_{42}(\eta)H_{a\rho}(\eta) &= B_{41}(\eta)H_{oz}(-m_2) + B_{42}(\eta)H_{o\rho}(-m_2)
\end{aligned} \tag{51}$$

where on the LHS we have plus field unknowns in η and on the RHS we have minus field unknowns in $m_i()$. The apparent redundancy in (51) after the imposition of boundary conditions is exploited to obtain integral representations only in terms of the field components $H_{oz}(\eta)$, $H_{o\rho}(\eta)$, $H_{az}(\eta)$, $H_{a\rho}(\eta)$ in the unique complex plane η using (49). Furthermore, the application of the novel version of the Fredholm factorization method allows us to obtain regularized integral equations. We assert that this procedure is applicable to GWHEs in general, not only for the specific problem presented in this simple example. The application of (49) to the RHS of (51) yields the following:

$$\begin{aligned}
A_{11}(\eta)H_{oz}(\eta) + A_{12}(\eta)H_{o\rho}(\eta) &= \tfrac{B_{11}(\eta)}{2\pi j}\int_{-\infty}^{\infty}\tfrac{H_{az}(\eta')}{\eta'+m_3}d\eta' + \tfrac{B_{12}(\eta)}{2\pi j}\int_{-\infty}^{\infty}\tfrac{H_{a\rho}(\eta')}{\eta'+m_3}d\eta' + H_{az}^{n.s}(-m_3) + H_{a\rho}^{n.s}(-m_3)\\
A_{21}(\eta)H_{oz}(\eta) + A_{22}(\eta)H_{o\rho}(\eta) &= \tfrac{B_{21}(\eta)}{2\pi j}\int_{-\infty}^{\infty}\tfrac{H_{az}(\eta')}{\eta'+m_4}d\eta' + \tfrac{B_{22}(\eta)}{2\pi j}\int_{-\infty}^{\infty}\tfrac{H_{a\rho}(\eta')}{\eta'+m_4}d\eta' + H_{az}^{n.s}(-m_4) + H_{a\rho}^{n.s}(-m_4)\\
A_{31}(\eta)H_{az}(\eta) + A_{32}(\eta)H_{a\rho}(\eta) &= \tfrac{B_{31}(\eta)}{2\pi j}\int_{-\infty}^{\infty}\tfrac{H_{oz}(\eta')}{\eta'+m_1}d\eta' + \tfrac{B_{32}(\eta)}{2\pi j}\int_{-\infty}^{\infty}\tfrac{H_{o\rho}(\eta')}{\eta'+m_1}d\eta' + H_{oz}^{n.s}(-m_1) + H_{o\rho}^{n.s}(-m_1)\\
A_{41}(\eta)H_{az}(\eta) + A_{42}(\eta)H_{a\rho}(\eta) &= \tfrac{B_{41}(\eta)}{2\pi j}\int_{-\infty}^{\infty}\tfrac{H_{az}(\eta')}{\eta'+m_2}d\eta' + \tfrac{B_{42}(\eta)}{2\pi j}\int_{-\infty}^{\infty}\tfrac{H_{a\rho}(\eta')}{\eta'+m_2}d\eta' + H_{oz}^{n.s}(-m_2) + H_{o\rho}^{n.s}(-m_2)
\end{aligned} \tag{52}$$

recalling that all occurrences of m_i are functions of η, i.e., $m_i(\eta)$. The integral equations in (52) are of the singular type; for this reason, we resort to the Fredholm factorization method to obtain regularized expressions. The procedure consists of γ_{1t} Cauchy *smile* contour integration [11] on both sides of each equation and consequent mathematical elaboration. Focusing our attention on the LHS for each term of each equation in (52), using dummy subscripts, we have the following regularized expression:

$$\begin{aligned}
\tfrac{1}{2\pi j}\int_{\gamma_{1t}}\tfrac{A(t)H_+(t)}{t-\eta}dt &= \tfrac{1}{2\pi j}\int_{\gamma_{1t}}\tfrac{(A(t)-A(\eta))H_+(t)}{t-\eta}dt + \tfrac{A(\eta)}{2\pi j}\int_{\gamma_{1t}}\tfrac{H_+(t)}{t-\eta}dt\\
&= \tfrac{1}{2\pi j}\int_{-\infty}^{\infty}\tfrac{(A(t)-A(\eta))H_+(t)}{t-\eta}dt + A(\eta)H_+(\eta) - A(\eta)H_+^{n.s}(\eta).
\end{aligned} \tag{53}$$

Focusing our attention on the RHS for each term of each equation in (52), using dummy subscripts and going back to the representation in (51), we have the following regularized expression:

$$\begin{aligned}\frac{1}{2\pi j}\int\limits_{\gamma_{1t}}\frac{B(t)H_+(-m(t))}{t-\eta}dt &= \frac{1}{2\pi j}\int\limits_{\gamma_{1t}}\frac{(B(t)-B(\eta))H_+(-m(t))}{t-\eta}dt + \frac{B(\eta)}{2\pi j}\int\limits_{\gamma_{1t}}\frac{H_+(-m(t))}{t-\eta}dt \\ = \frac{1}{(2\pi j)^2}\int\limits_{-\infty}^{\infty}\int\limits_{-\infty}^{\infty}\frac{(B(t)-B(\eta))H_+(\eta')}{(t-\eta)(\eta'+m(t))}dt\,d\eta' &+ \frac{B(\eta)}{(2\pi j)^2}\int\limits_{-\infty}^{\infty}\int\limits_{\gamma_{1t}}\frac{1}{(t-\eta)(\eta'+m(t))}dtH_+(\eta')d\eta' + n.s.\,terms.\end{aligned} \tag{54}$$

Given the expressions of $m_i(\eta)$ in (24)–(25) with $Im[m_i(t)] < 0$ in lossy media (Figure 4), Equation (54) requires the computation of

$$M_e(\eta,\eta') = \int\limits_{\gamma_{1t}}\frac{1}{(t-\eta)(\eta'+m(t))}dt, \tag{55}$$

which can be performed either numerically or analytically while paying attention to the branch cuts of $m(t)$. Furthermore, in (54) we also need to consider n.s. singularities related to the field.

The validity of the estimation of $M_e(\eta,\eta')$ extends to complex values of η' as long as η' does not cross the singularity line determined by the behavior of $-m(t)$ for $t \in \mathbb{R}$, as shown in Figure 4.

The expressions in (53) and (54) are regularized integral terms, as their kernels are compact. Moreover, they include the n.s. terms of the field components in η and $-m_i$, respectively. The detailed proof of this assertion needs to be performed for specific problems. While numerically implementing the method we observe that one of the main difficulties resides in the correct estimation of kernel functions $A(\eta), B(\eta)$ for the presence of multivalued functions that need particular attention in their definition and calculation.

For simplicity and compactness of discussion, we examine the properties of integral equations in the simple case of a PEC wedge immersed in an isotropic medium in Section 5.2. Equation (51) yields a 4×4 system of Fredholm integral equations of the second kind by utilizing (52), (53), and (54). This system is expressed in terms of $H_{oz}(\eta)$, $H_{o\rho}(\eta)$, $H_{az}(\eta)$, $H_{a\rho}(\eta)$. It is important to highlight that the system only depends on the spectral variable η, ensuring that functions do not rely on m_i outside of the integration sign. This property is fundamental to avoid the analysis of unknowns defined in different complex planes (η and various m_i) that are correlated through cumbersome improper sheet properties.

4. Asymptotic Estimation of the Field in the Angular Region

Having obtained the spectra at the faces of the angular region, we can estimate the asymptotic behavior of the far field inside of the angular region.

Going back to the solution of (26) in Section 2 for region 1, according to (28) we have

$$\tilde{\boldsymbol{\psi}}_{\boldsymbol{y}}(\eta,v) = \sum_{i=1}^{2} C_i e^{-\lambda_{\gamma i}(\gamma)\,v}\boldsymbol{u_i} + \sum_{i=3}^{4}\boldsymbol{u_i}\boldsymbol{v_i}\cdot\int\limits_{v}^{\infty} e^{-\lambda_{\gamma i}(\gamma)(v-v')}\boldsymbol{\psi_{sa}}(v')dv',\ v>0. \tag{56}$$

From the homogeneous portion of the solution in (56), we obtain the definitions of arbitrary coefficients in terms of the field components at $v = 0$ (face o):

$$\boldsymbol{v_i}\cdot\tilde{\boldsymbol{\psi}}_{\boldsymbol{y}}(\eta,0) = C_i,\ i=1,2. \tag{57}$$

The particular integrals in (56) are terms related to face a via $\boldsymbol{\psi_{sa}}(v)$. Due to the linearity of the problem, we apply the superposition principle; we can interpret (56) as the result of an equivalent theorem, where $\tilde{\boldsymbol{\psi}}_{\boldsymbol{y}}(\eta,v)$ is represented through equivalent sources at faces o

and a. Similarly, the spectral field in region 1 can be considered as a result of the analysis of the rotated region $2'$ from Figure 2b in Section 3, yielding

$$-\frac{d}{dv}\tilde{\boldsymbol{\psi}}_{\boldsymbol{Y_1}}(\eta, v) = \boldsymbol{M}_{\boldsymbol{\pi-\gamma}}(-j\alpha_o, -j\eta)\cdot\tilde{\boldsymbol{\psi}}_{\boldsymbol{Y_1}}(\eta, v) + \boldsymbol{\psi}_{\boldsymbol{so}}(v),\ v<0, \tag{58}$$

where we note that $\gamma \to \pi-\gamma$ impacts all terms of the solution, as already reported in Section 3, i.e., $\boldsymbol{u}_{\boldsymbol{iY_1}}$, $\boldsymbol{v}_{\boldsymbol{iY_1}}$, λ_{iY_1}, m_{iY_1}, and the field components. The solution takes the form

$$\tilde{\boldsymbol{\psi}}_{\boldsymbol{Y1}}(\eta, v) = \sum_{i=3}^{4} C_i e^{-\lambda_{\gamma iY_1}(\pi-\gamma)\,v}\boldsymbol{u}_{\boldsymbol{iY_1}} - \sum_{i=1}^{2}\boldsymbol{u}_{\boldsymbol{iY_1}}\boldsymbol{v}_{\boldsymbol{iY_1}}\cdot\int_{v}^{\infty} e^{-\lambda_{\gamma iY_1}(\pi-\gamma)(v-v')}\boldsymbol{\psi}_{\boldsymbol{so}}(v')dv',\ v<0, \tag{59}$$

where $v=-x$ in Figure 2b is now different from $v=X_1$ in Figure 2a. From the homogeneous portion of the solution in (59), we obtain the definitions of arbitrary coefficients in terms of the field components at $v=0$ (face a):

$$\boldsymbol{v}_{\boldsymbol{iY_1}}\cdot\tilde{\boldsymbol{\psi}}_{\boldsymbol{Y1}}(\eta, 0) = C_i,\ i=3,4. \tag{60}$$

The particular integrals in (59) are terms related to face o via $\boldsymbol{\psi}_{\boldsymbol{so}}(v)$. Due to the linearity of the problem, we again apply the superposition principle and can interpret (59) as the result of an equivalent theorem, where $\tilde{\boldsymbol{\psi}}_{\boldsymbol{Y1}}(\eta, v)$ is represented through equivalent sources at faces a and o.

Using the superposition principle and considering only homogeneous portions of (56) and (59), we can represent the complete field without the particular integrals. Each contribution originating from (56) and (59) is a spectral component that can be inversely Fourier/Laplace transformed into the physical domain (u, v); these contributions represent the fields from equivalent currents distributed in half-planes (face o and face a, respectively). The application of the asymptotic representation of fields for each component in a unique global system of cylindrical coordinates provides the estimation of the field in terms of the classical GTD for angular region 1, but as a superposition of the GTD for two half-planes (face o and face a), as in Kirchhoff representations. This procedure will be examined in detail in the practical examples reported in the following sections and is a fundamental tool for estimating the GTD directly in the Fourier/Laplace domain for an angular region filled by arbitrarily linear media, where the GTD in the w plane is not available (as is common in isotropic angular region problems). Indeed, the computation of the GTD for an angular region filled by arbitrarily linear media is proposed here by effectively resorting to the computation of the GTD in two half-plane problems.

An alternative way to obtain the far field is based on the computation of the spectral field for any azimuthal direction φ by splitting the angular region into two subregions at any observation angle φ (subregion A $0<\varphi'<\varphi$ and subregion B $\varphi<\varphi'<\gamma$). After the face spectra at $\varphi=0, \gamma$ have been obtained for the entire angular region, as proposed in the previous sections, we can then relate the spectra at φ to those of the two faces using the functional equations of the two subregions. These φ-parametric spectral representations of field spectra allow for asymptotic evaluation of the far field at any φ. We observe that the functional equations are written in terms of continuous field components at the boundary faces of the angular region; see Section 4. The properties analyzed in this section can be interpreted as *a novel and original form of the electromagnetic equivalence theorem in the spectral domain in the specific context of problems involving angular regions filled by an arbitrary linear medium.*

5. Validation of the Novel Regularization Procedure with a Simple Example: Direct Fredholm Factorization Applied to a PEC Wedge in an Isotropic Region

In order to validate the procedure from a mathematical point of view, let us first demonstrate its efficacy in the simple case of angular region 1 (Figure 2a,b), representing a PEC wedge filled by an isotropic medium, where a closed-form WH solution is available. From the following:

$$m = m_i(\pi - \gamma) = m_{i+2}(\gamma) = -\eta\cos\gamma + \xi\sin\gamma\ ,\ i = 1,2;\ \xi = \sqrt{k^2 - \alpha_o^2 - \eta^2} \tag{61}$$

$$\boldsymbol{u_1} = \begin{vmatrix} \frac{\tau_o^2}{\omega\,\varepsilon\,\xi} \\ -\frac{\alpha_o\eta}{\omega\,\varepsilon\,\xi} \\ 0 \\ 1 \end{vmatrix},\ \boldsymbol{u_2} = \begin{vmatrix} \frac{\alpha_o\eta}{\omega\,\varepsilon\,\xi} \\ -\frac{(\xi^2+\alpha_o^2)}{\omega\,\varepsilon\,\xi} \\ 1 \\ 0 \end{vmatrix},\ \boldsymbol{u_3} = \begin{vmatrix} -\frac{\tau_o^2}{\omega\,\varepsilon\,\xi} \\ \frac{\alpha_o\eta}{\omega\,\varepsilon\,\xi} \\ 0 \\ 1 \end{vmatrix},\ \boldsymbol{u_4} = \begin{vmatrix} -\frac{\alpha_o\eta}{\omega\,\varepsilon\,\xi} \\ \frac{(\xi^2+\alpha_o^2)}{\omega\,\varepsilon\,\xi} \\ 1 \\ 0 \end{vmatrix} \tag{62}$$

$$\begin{aligned} \boldsymbol{v_1} &= \begin{vmatrix} \frac{\xi^2+\alpha_o^2}{2\omega\,\mu\,\xi} & \frac{\alpha_0\eta}{2\omega\,\mu\,\xi} & 0 & \frac{1}{2} \end{vmatrix}, \boldsymbol{v_2} = \begin{vmatrix} -\frac{\alpha_0\eta}{2\omega\,\mu\,\xi} & -\frac{k^2-\alpha_o^2}{2\omega\,\mu\,\xi} & \frac{1}{2} & 0 \end{vmatrix} \\ \boldsymbol{v_3} &= \begin{vmatrix} -\frac{\xi^2+\alpha_o^2}{2\omega\,\mu\,\xi} & -\frac{\alpha_0\eta}{2\omega\,\mu\,\xi} & 0 & \frac{1}{2} \end{vmatrix}, \boldsymbol{v_4} = \begin{vmatrix} \frac{\alpha_0\eta}{2\omega\,\mu\,\xi} & \frac{k_o^2-\alpha_o^2}{2\omega\,\mu\,\xi} & \frac{1}{2} & 0 \end{vmatrix} \end{aligned} \tag{63}$$

we have the functional equations [34] for region 1 (the first two equations in (45)):

$$\begin{aligned} &-\alpha_o\eta E_{o\rho}(\eta) + (\eta^2 - k^2)E_{oz}(\eta) + k\xi Z_o H_{o\rho}(\eta) \\ &= -\alpha_o\eta E_{a\rho}(-m) - [\eta\xi\sin(\gamma) + \cos(\gamma)(k^2 - \eta^2)]E_{az}(-m) \\ &+k\xi Z_o H_{a\rho}(-m) - \sin(\gamma)\alpha_o k Z_o H_{az}(-m) \end{aligned} \tag{64}$$

$$\begin{aligned} &(k^2 - \alpha_o^2)E_{o\rho}(\eta) + \alpha_o\eta E_{oz}(\eta) + k\xi Z_o H_{oz}(\eta) \\ &= (k^2 - \alpha_o^2)E_{a\rho}(-m) + \alpha_o[\cos(\gamma)\eta - \sin(\gamma)\xi]E_{az}(-m) \\ &+kZ_o[\sin(\gamma)\eta + \cos(\gamma)\xi]H_{az}(-m). \end{aligned} \tag{65}$$

At normal incidence ($\alpha_o = 0$), we obtain

$$-\xi E_{oz}(\eta) + kZ_o H_{o\rho}(\eta) = -[\eta\sin(\gamma) + \xi\cos(\gamma)]E_{az}(-m) + kZ_o H_{a\rho}(-m), \tag{66}$$

$$kE_{o\rho}(\eta) + \xi Z_o H_{oz}(\eta) = kE_{a\rho}(-m) + Z_o[\eta\sin(\gamma) + \xi\cos(\gamma)]H_{az}(-m), \tag{67}$$

where we note the decoupling of Equations (66) and (67) for E_z and H_z polarization, respectively. The imposition of the PEC boundary conditions on functional Equations (66) and (67) yields the GWHEs

$$H_{o\rho}(\eta) = H_{a\rho}(-m), \tag{68}$$

$$\xi H_{oz}(\eta) = [\eta\sin(\gamma) + \xi\cos(\gamma)]H_{az}(-m), \tag{69}$$

with plus/minus field unknowns, respectively, in η, m. We note that the regularity properties of the problem depend on the multivalued function $\xi = \sqrt{k^2 - \eta^2}$ (due to physical reasons) [11], which defines proper and improper sheets of the η plane.

5.1. Classical Solution of the GWHEs of the Problem in Different Complex Planes

In order to illustrate and validate the new direct Fredholm factorization procedure of Section 3 in the following subsections, this subsection presents the classical WH solution of (68) and (69) obtained in closed form [11] with the help of a specialized mapping, factorization, and decomposition and with the extraction of source terms such as geometrical optics (GO) fields for plane wave illumination. This subsection also clarifies important properties related to different complex planes (including the angular complex plane w) where the problem and the solutions are represented.

The specialized mapping for the closed-form WH solution is

$$\eta = -k\cos\left(\frac{\gamma}{\pi}\arccos\left(-\frac{\bar{\eta}}{k}\right)\right), \tag{70}$$

which was introduced for the first time in 2001 and has been extensively used in isotropic wedge scattering problems, as reported in [11,12]. The mapping transforms plus unknowns in the η plane and minus unknowns in the m plane (61) into plus and minus unknowns in the $\bar{\eta}$ plane, respectively, yielding the following classical Wiener–Hopf equations in the new complex plane $\bar{\eta}$:

$$H_{o\rho+}(\bar{\eta}) = H_{a\rho+}(-\bar{\eta}) \tag{71}$$

$$\xi H_{oz+}(\bar{\eta}) = [\eta\sin(\gamma) + \xi\cos(\gamma)]H_{az+}(-\bar{\eta}) \tag{72}$$

where ξ and η become functions of $\bar{\eta}$ and

$$m = k\cos\left(\frac{\gamma}{\pi}\arccos\left(-\frac{\bar{\eta}}{k}\right) + \gamma\right). \tag{73}$$

From this point, the solution proceeds as it does for CWHEs, with factorization, decomposition, and the application of Liouville's theorem while considering plane wave illumination with E_z and H_z polarization and incident waves.

$$E_z^i(\rho,\varphi) = E_o e^{jk\rho\cos(\varphi-\varphi_o)},\ H_\rho^i(\rho,\varphi) = -\frac{1}{j\omega\mu\rho}\frac{\partial E_z^i(\rho,\varphi)}{\partial\varphi} = \frac{k}{\omega\ \mu}\sin(\varphi-\varphi_o)e^{jk\rho\cos(\varphi-\varphi_o)}E_o \tag{74}$$

$$H_z^i(\rho,\varphi) = H_o e^{jk\rho\cos(\varphi-\varphi_o)},\ E_\rho^i(\rho,\varphi) = \frac{1}{j\omega\varepsilon\rho}\frac{\partial H_z^i(\rho,\varphi)}{\partial\varphi} = -\frac{k}{\omega\varepsilon}\sin(\varphi-\varphi_o)e^{jk\rho\cos(\varphi-\varphi_o)}H_o \tag{75}$$

Due to the PEC boundary conditions, we obtain the following GO source terms, which are tangential to faces a and o, respectively, of angular region 1.

$$H_x^{GO}(\rho,0) = -2\frac{E_o}{Z_o}\sin\varphi_o e^{jk\rho\cos\varphi_o},\ H_\rho^{GO}(\rho,\gamma) = 2\frac{E_o}{Z_o}\sin(\gamma-\varphi_o)e^{jk\rho\cos(\gamma-\varphi_o)} \tag{76}$$

$$H_z^{GO}(\rho,0) = 2H_o e^{jk\rho\cos(\varphi_o)},\ H_z^{GO}(\rho,\gamma) = 2H_o e^{jk\rho\cos(\gamma-\varphi_o)} \tag{77}$$

In the spectral domain, according to the Laplace transforms (33)–(34), (76)–(77) become

$$H_{o\rho}^{GO}(\eta) = \frac{-2jE_o\sin\varphi_o}{Z_o(\eta-\eta_o)},\ H_{a\rho}^{GO}(-m) = \frac{-2jE_o\sin(\gamma-\varphi_o)}{Z_o(m-m_o)} \tag{78}$$

$$H_{oz}^{GO}(\eta) = \frac{2jH_o}{\eta-\eta_o},\ H_{az}^{GO}(-m) = \frac{-2jH_o}{m-m_o} \tag{79}$$

with $\eta_o = -k\cos\varphi_o$ and $m_o = k\cos(\gamma-\varphi_o)$. In the $\bar{\eta}$ plane (70), pole η_o is mapped into $\bar{\eta}_o = -k\cos(-\frac{\pi}{\gamma}\varphi_o)$. In the following, we assume $\varphi_o < \gamma/2$ to locate $\bar{\eta}_o$ in the upper half-plane of the complex plane $\bar{\eta}$, yielding non-standard plus unknowns; generalization is straightforward, yielding $\bar{\eta}_o$ in the $\bar{\eta}$-lower half-plane, while $\gamma/2 < \varphi_o < \gamma$.

Focusing our attention on E_z polarization, due to the simplicity of Equation (71), we observe the absence of a need for factorization; thus, we perform decomposition to highlight the non-standard contribution in the plus unknown $H_{o\rho+}(\bar{\eta})$, which is constituted by $H_{o\rho}^{GO}(\eta) = R/(\eta-\eta_o)$ (78) and can be mapped into the $\bar{\eta}$ plane (70), yielding $H_{o\rho}^{GO}(\bar{\eta}) = T/(\eta-\eta_o)$. We obtain

$$H_{o\rho+}(\bar{\eta}) - \frac{T}{\bar{\eta}-\bar{\eta}_o} = H_{a\rho+}(-\bar{\eta}) - \frac{T}{\bar{\eta}-\bar{\eta}_o} \tag{80}$$

with

$$T = R\left.\frac{d\bar{\eta}}{d\eta}\right|_{\eta_o} = -2j\frac{\pi}{\gamma}\frac{E_o}{Z_o}\sin\frac{\pi}{\gamma}\varphi_o,\ R = \frac{-2jE_o\sin\varphi_o}{Z_o},\ \left.\frac{d\bar{\eta}}{d\eta}\right|_{\eta_o} = \frac{\pi}{\gamma}\frac{\sin\frac{\pi}{\gamma}\varphi_o}{\sin\varphi_o}. \tag{81}$$

Due to the regularity and asymptotic behavior of the LHS and RHS of (80), applying Liouville's theorem, (80) is equal to zero; thus, we obtain the following simple closed-form solutions:

$$H_{o\rho+}(\bar{\eta}) = \frac{T}{\bar{\eta}-\bar{\eta}_o},\quad H_{a\rho+}(\bar{\eta}) = -\frac{T}{\bar{\eta}+\bar{\eta}_o}. \tag{82}$$

The solutions in (82) can be mapped into the η plane using the inverse mapping of (70):

$$\bar{\eta} = -k\cos\left(\frac{\pi}{\gamma}\arccos\left(-\frac{\eta}{k}\right)\right). \tag{83}$$

We recall that the regularity properties of the problem in (68)–(69) in the η plane depend on the multivalued function $\xi = \sqrt{k^2-\eta^2}$ (due to physical reasons), and now, after the application of the mapping in (70), on the multivalued function $\kappa = \sqrt{k^2-\bar{\eta}^2}$ in the $\bar{\eta}$ plane through the log representation of $\arccos(-\bar{\eta}/k)$; see Section 3.4 of [11]. Contrary to (70), the transformation in (83) requires particular attention, as it maps $\bar{\eta}$ into η for $0 < \gamma < \pi$ without covering the entire proper sheet of the η plane defined by the ξ function. For this reason, a portion of the proper sheet of the η plane falls into the improper sheet of the $\bar{\eta}$ plane (defined by κ), and because the closed-form solution is obtained in the $\bar{\eta}$ plane, this solution must be considered correct (not offending) only in the proper sheet of $\bar{\eta}$ even after applying the transformation in (83). To easily control the proper/improper sheets of the η and $\bar{\eta}$ planes, we can resort to their visualization in the complex plane w ($\eta = -k\cos w$; thus, $\bar{\eta} = -k\cos\left(\frac{\pi}{\gamma}w\right)$ and $m = k\cos(w+\gamma)$). The w plane shows the proper sheets of both planes $(\eta, \bar{\eta})$ in a unique plane. In particular, for real w, the proper segments originating from η and $\bar{\eta}$ (related to ξ and κ, respectively) are $-\pi < w < 0$ and $-\gamma < w < 0$, respectively; see Section 3.4 of [11]. This means that the closed-form solution obtained in the proper sheet of $\bar{\eta}$ is not valid in the entire proper sheet of the η plane but only in a portion, which is due to the properties of (83).

Let us now consider the CWHE of H_z polarization (72)

$$G(\bar{\eta})H_{oz+}(\bar{\eta}) = H_{az+}(-\bar{\eta}),\ G(\bar{\eta}) = \xi/n, \tag{84}$$

with $n = -\eta\sin(\gamma) - \xi\cos(\gamma) = \sqrt{k^2-m^2}$. According to [33], we have the factorization

$$G_-(\bar{\eta}) = \frac{G(\bar{\eta})}{G_+(\bar{\eta})},\ G_+(\bar{\eta}) = \frac{\xi}{\xi_- n_+},\ \xi_- = \sqrt{k-\bar{\eta}},\ n_+ = \sqrt{k+\bar{\eta}}. \tag{85}$$

Confirming the same assumption that $\varphi_o < \gamma/2$ for simplicity, $\bar{\eta}_o$ is located in the $\bar{\eta}$ upper half-plane, yielding a nonstandard plus unknown $H_{oz+}(\bar{\eta})$ that is constituted by the source nonstandard component $H_{oz}^{GO}(\eta) = R_H/(\eta-\eta_o)$ (79), which in the $\bar{\eta}$ plane becomes

$$H_{oz}^{GO}(\bar{\eta}) = \frac{T_H}{\bar{\eta}-\bar{\eta}_o},\ T_H = R_H\left.\frac{d\bar{\eta}}{d\eta}\right|_{\eta_o} = 2jH_o\frac{\pi}{\gamma}\frac{\sin\frac{\pi}{\gamma}\varphi_o}{\sin\varphi_o},\ R_H = 2jH_o. \tag{86}$$

Applying factorization and decomposition to (84), we obtain

$$G_+(\bar{\eta})H_{oz+}(\bar{\eta}) - G_+(\bar{\eta}_o)H_{oz}^{GO}(\bar{\eta}) = G_-^{-1}(\bar{\eta})H_{az+}(-\bar{\eta}) - G_+(\bar{\eta}_o)H_{oz}^{GO}(\bar{\eta}). \tag{87}$$

Due to the regularity and asymptotic behavior of the LHS and RHS of (87), applying Liouville's theorem, (87) is equal to zero; thus, we obtain the following simple closed-form solutions:

$$H_{oz+}(\bar{\eta}) = G_+^{-1}(\bar{\eta})G_+(\bar{\eta}_o)H_{oz}^{GO}(\bar{\eta}),\ H_{az+}(-\bar{\eta}) = G_-(\bar{\eta})G_+(\bar{\eta}_o)H_{oz}^{GO}(\bar{\eta}). \tag{88}$$

Again, the closed-form solutions in (88) with the H_z polarization obtained in the proper sheet of the $\bar{\eta}$ plane can be mapped into the η plane using the inverse mapping in (83); however, we need to consider these solutions valid only for η values belonging to the proper sheet of the $\bar{\eta}$ plane. Moreover, this property can be ascertained by checking that (68)–(69) (from which we obtained the solutions in $\bar{\eta}$) are enforced only for η values belonging to the proper sheet of the $\bar{\eta}$ plane.

In order to obtain solutions that are valid in the entire proper sheet of the η plane or beyond (i.e., also in the improper sheet), we need to resort to an analytical continuation technique that, in case of a unique propagation constant problems, can be implemented via representation of GWHEs in the complex w plane yielding difference equations (for instance, see the examples in [11,12]). Another option is to describe the problem with a unique propagation constant directly in the w plane, where the concept of proper and improper sheets of the η and $\bar{\eta}$ planes is expanded periodically into the w plane with an alternative vision of Riemann sheets. In this case, the closed-form solutions corresponding to (88) and (89) are valid in the entire w plane, as opposed to approximate solutions obtained with numerical line integration located in a particular sheet in either the $\bar{\eta}$ or w plane. In this last case, which originates from the classical implementation of Fredholm factorization [12], we again need to resort to difference equations for analytical continuation.

$$H_{oz+}(w) = \frac{2jH_o\pi\csc w\sin\frac{\pi w}{\gamma}}{-k\gamma\cos\frac{\pi w}{\gamma}+k\gamma\cos\frac{\pi\varphi_o}{\gamma}},\ H_{az+}(w) = -\frac{2jH_o\pi\csc w\sin\frac{\pi w}{\gamma}}{k\gamma\cos\frac{\pi w}{\gamma}+k\gamma\cos\frac{\pi\varphi_o}{\gamma}} \tag{89}$$

5.2. Regularized Integral Equation Method for the Direct Solution of the GWHEs in Angular Regions (Direct Fredholm Factorization)

Following the procedure in Section 3, which is simplified in the current problem because of the isotropic medium, we duplicate the equations. For E_z polarization, we have

$$\begin{aligned} H_{o\rho}(\eta) &= H_{a\rho}(-m),\\ H_{a\rho}(\eta) &= H_{o\rho}(-m), \end{aligned} \tag{90}$$

while for H_z polarization, we have

$$\begin{aligned} \xi H_{oz}(\eta) &= [\eta\sin(\gamma)+\xi\cos(\gamma)]H_{az}(-m)\\ \xi H_{az}(\eta) &= [\eta\sin(\gamma)+\xi\cos(\gamma)]H_{oz}(-m) \end{aligned} \tag{91}$$

where $m = m(\eta)$ is defined in (61). Notice that when applying (70) to each of (90)–(91), the duplicated equations assume the same form of the original ones (both CWHEs), with only the replacement of $\bar{\eta}$ with $-\bar{\eta}$.

Both systems of equations can be considered a particular case of

$$\begin{aligned} G(\eta)F_+(\eta) &= H(\eta)X_+(-m)\\ G_a(\eta)X_+(\eta) &= H_a(\eta)F_+(-m) \end{aligned} \tag{92}$$

which is suitable for describing more general cases. To describe the procedure, for simplicity, let us assume that $F_+(\eta)$ is a non-standard plus η unknown while $X_+(-m)$ is a standard minus m unknown; generalization is possible with a little effort.

Applying the Cauchy decomposition Formula (49) to the unknowns defined in $-m(\eta)$,

$$\begin{aligned} F_+(-m) &= \tfrac{1}{2\pi j}\int\limits_{-\infty}^{\infty}\tfrac{F_+(\eta')}{\eta'+m}d\eta' + F_+^{n.s.}(-m),\ \eta\in\mathbb{R} \\ X_+(-m) &= \tfrac{1}{2\pi j}\int\limits_{-\infty}^{\infty}\tfrac{X_+(\eta')}{\eta'+m}d\eta',\ \eta\in\mathbb{R}. \end{aligned} \tag{93}$$

From (92), we obtain the following system of integral equations:

$$\begin{aligned} G(\eta)F_+(\eta) &= \tfrac{1}{2\pi j}H(\eta)\int\limits_{-\infty}^{\infty}\tfrac{X_+(\eta')}{\eta'+m(\eta)}d\eta' \\ G_a(\eta)X_+(\eta) &= \tfrac{1}{2\pi j}H_a(\eta)\int\limits_{-\infty}^{\infty}\tfrac{F_+(\eta')}{\eta'+m(\eta)}d\eta' + H_a(\eta)F_+^{n.s.}(-m(\eta)). \end{aligned} \tag{94}$$

This is not a system of Fredholm integral equations of the second kind (non-compact kernel). To regularize (94), we follow the procedure presented in Section 3. Performing a smile integration of (94), after mathematical manipulation, on the LHS, we have

$$\begin{aligned} \tfrac{1}{2\pi j}\int\limits_{\gamma_{1t}}\tfrac{G(t)F_+(t)}{t-\eta}dt &= G(\eta)F_+(\eta) + \tfrac{1}{2\pi j}\int\limits_{-\infty}^{\infty}\tfrac{(G(t)-G(\eta))F_+(t)}{t-\eta}dt - G(\eta)F_+^{ns}(\eta) \\ \tfrac{1}{2\pi j}\int\limits_{\gamma_{1t}}\tfrac{G_a(t)X_+(t)}{t-\eta}dt &= G_a(\eta)X_+(\eta) + \tfrac{1}{2\pi j}\int\limits_{-\infty}^{\infty}\tfrac{(G_a(t)-G_a(\eta))X_+(t)}{t-\eta}dt \end{aligned} \tag{95}$$

and on the RHS we have

$$\frac{1}{2\pi j}\int\limits_{\gamma_{1t}}\frac{1}{2\pi j}\frac{H(t)}{t-\eta}\int\limits_{-\infty}^{\infty}\frac{X_+(\eta')}{\eta'+m(t)}d\eta'dt = \frac{1}{(2\pi j)^2}\int\limits_{-\infty}^{\infty}M(\eta,\eta')X_+(\eta')d\eta' \tag{96}$$

and

$$\begin{aligned} \tfrac{1}{2\pi j}\int\limits_{\gamma_{1t}}\tfrac{1}{2\pi j}\tfrac{H_a(t)}{t-\eta}\int\limits_{-\infty}^{\infty}\tfrac{F_+(\eta')}{\eta'+m(t)}d\eta'dt &= \tfrac{1}{(2\pi j)^2}\int\limits_{-\infty}^{\infty}M_a(\eta,\eta')F_+(\eta')d\eta' \\ \tfrac{1}{2\pi j}\int\limits_{\gamma_{1t}}\tfrac{H_a(t)}{t-\eta}F_+^{ns}(-m(t))dt &= \tfrac{1}{2\pi j}\int\limits_{-\infty}^{\infty}\tfrac{[H_a(t)-H_a(\eta)]F_+^{ns}(-m(t))}{t-\eta}dt + \tfrac{H_a(\eta)}{2\pi j}\int\limits_{\gamma_{1t}}\tfrac{F_+^{ns}(-m(t))}{t-\eta}dt \end{aligned} \tag{97}$$

where

$$\begin{aligned} M(\eta,\eta') &= \int\limits_{\gamma_{1t}}\tfrac{H(t)}{(t-\eta)(\eta'+m(t))}dt = \int\limits_{-\infty}^{\infty}\tfrac{H(t)-H(\eta)}{(t-\eta)(\eta'+m(t))}dt + H(\eta)\int\limits_{\gamma_{1t}}\tfrac{1}{(t-\eta)(\eta'+m(t))}dt \\ M_a(\eta,\eta') &= \int\limits_{\gamma_{1t}}\tfrac{H_a(t)}{(t-\eta)(\eta'+m(t))}dt = \int\limits_{-\infty}^{\infty}\tfrac{H_a(t)-H_a(\eta)}{(t-\eta)(\eta'+m(t))}dt + H_a(\eta)\int\limits_{\gamma_{1\eta}}\tfrac{1}{(t-\eta)(\eta'+m(t))}dt. \end{aligned} \tag{98}$$

Merging (95) and (96)–(98), we obtain the following FIEs of the second kind:

$$G(\eta)F_+(\eta) + \frac{1}{2\pi j}\int\limits_{-\infty}^{\infty}\frac{(G(t)-G(\eta))F_+(t)}{t-\eta}dt = \frac{1}{(2\pi j)^2}\int\limits_{-\infty}^{\infty}M(\eta,\eta')X_+(\eta')d\eta' + G(\eta))F_+^{ns}(\eta) \tag{99}$$

$$\begin{aligned} &G_a(\eta)X_+(\eta) + \tfrac{1}{2\pi j}\int\limits_{-\infty}^{\infty}\tfrac{(G_a(t)-G_a(\eta))X_+(t)}{t-\eta}dt \\ &= \tfrac{1}{(2\pi j)^2}\int\limits_{-\infty}^{\infty}M_a(\eta,\eta')F_+(\eta')d\eta' + \tfrac{1}{2\pi j}\int\limits_{-\infty}^{\infty}\tfrac{(H_a(t)-H_a(\eta))F_+^{ns}(-m(t))}{t-\eta}dt + \tfrac{H_a(\eta)}{2\pi j}\int\limits_{\gamma_{1t}}\tfrac{F_+^{ns}(-m(t))}{t-\eta}dt. \end{aligned} \tag{100}$$

It can be observed that the regularized FIEs (99) and (100) are particularly efficient from a computational point of view due to the presence of compact kernels integrated along the real axis, with the exception of the smile integration included in (98):

$$M_e(\eta,\eta') = \int\limits_{\gamma_{1t}} \frac{1}{(t-\eta)(\eta'+m(t))}dt. \tag{101}$$

The evaluation of the integral in (101) can be effectively performed by warping the *smile* contour γ_{1t} in the lower half of the complex t plane into the integration path λ_1 wrapped around the vertical branch cut Γ_1 of $m(t)$ (61), which originated in branch point $+k$ (see Figure 5).

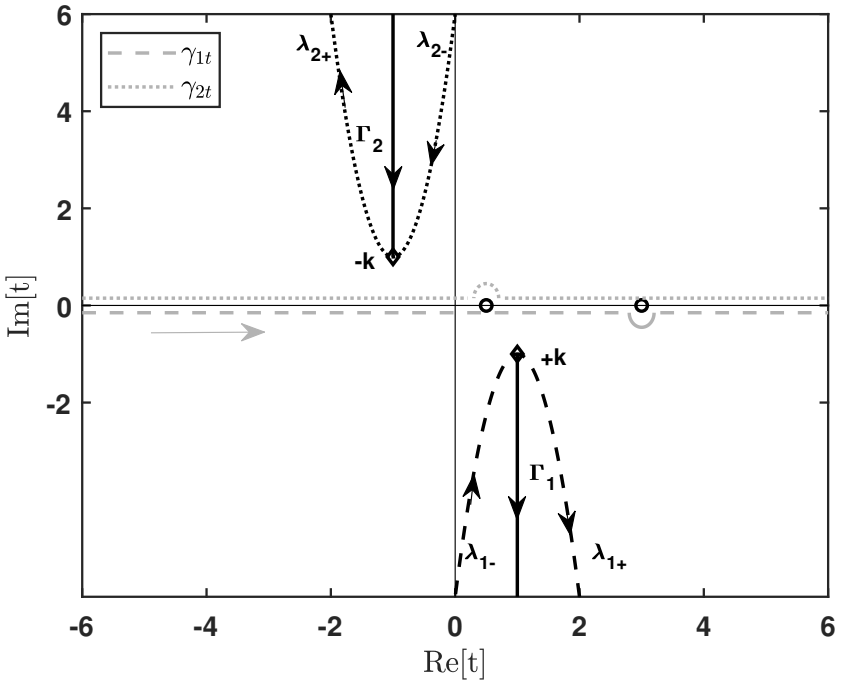

Figure 5. Vertical branch cuts $\Gamma_{1,2}$ of $m(t)$ originating in branch point $\pm k$ assuming a lossy medium (for visibility, $k = 1 - j$), *smile* contour integration line γ_{1t}, and *frown* contour integration line γ_{2t} with corresponding warped contours λ_1 and λ_2 wrapped around vertical branch cuts Γ_1 and Γ_2. Note that γ_{1t} and γ_{2t} assume different observation points for indentation in the figure.

By collapsing λ_1 onto Γ_1, we obtain

$$M_e(\eta,\eta') = \int_{\Gamma_1} \Delta(\frac{1}{(t-\eta)(\eta'+m(t)}) dt, \tag{102}$$

where

$$\Delta(\frac{1}{(t-\eta)(\eta'+m(t)}) = -\frac{4\sqrt{(k-t)(k+t)}\sin(\gamma)}{(t-\eta)[-k^2+2(t^2+\eta'^2)-4t\eta'\cos(\gamma)+k^2\cos(2\gamma)]}. \tag{103}$$

Assuming that $t = k - jv$ $(v > 0)$, the representation in (102) is quickly numerically convergent. A closed-form expression of (102) is obtainable by considering the following:

1. Selection of the branch cut Γ_1 as the line $t = ku$ (with real $u > 1$) replacing λ_1 and use of the mapping $t = ku$ under the integration sign.
2. Expansion of (103) with a minimal denominator.
3. Careful mathematical manipulation of multivalued functions.

We obtain

$$M_e(\eta,\eta') = -2\sin(\gamma)\left(\frac{F_\infty(u_1(\eta))}{(u_1(\eta)-u_2(\eta'))(u_1(\eta)-u_3(\eta'))} - \frac{F_\infty(u_2(\eta'))}{(u_1(\eta)-u_2(\eta'))(u_2(\eta')-u_3(\eta'))} + \frac{F_\infty(u_3(\eta'))}{(u_1(\eta)-u_3(\eta'))(u_2(\eta')-u_3(\eta'))}\right) \tag{104}$$

with

$$F_\infty(u) = ju\log(2) - \sqrt{1-u^2}\log(-u + j\sqrt{1-u^2}) \tag{105}$$

and the poles

$$u_1(\eta) = \eta/k,\ u_2(\eta') = \frac{\eta'\cos\gamma - \sqrt{k^2-\eta'^2}\sin\gamma}{k},\ u_3(\eta') = \frac{\eta'\cos\gamma + \sqrt{k^2-\eta'^2}\sin\gamma}{k}. \tag{106}$$

Let us now go back to particular cases and consider equations for H_z polarization (91) in angular region 1 representing a PEC wedge, written in the form (92) with the following definitions:

$$F_+(\eta) = H_{oz}(\eta),\ X_+(\eta) = H_{az}(\eta),\ G(\eta) = G_a(\eta) = \frac{\xi}{\eta\sin(\gamma) + \xi\cos(\gamma)},\ H(\eta) = H_a(\eta) = 1. \tag{107}$$

The set of FIEs (99)–(100) is simplified; in particular, $M(\eta,\eta') = M_a(\eta,\eta') = M_e(\eta,\eta')$, as reported in (102). Equations (99)–(100) respectively become the following system of FIEs:

$$G(\eta)H_{oz}(\eta) + \frac{1}{2\pi j}\int_{-\infty}^{\infty}\frac{(G(t)-G(\eta))H_{oz}(t)}{t-\eta}dt = \frac{1}{(2\pi j)^2}\int_{-\infty}^{\infty}M_e(\eta,\eta')H_{az}(\eta')d\eta' + s_1(\eta) \tag{108}$$

and

$$G(\eta)H_{az}(\eta) + \frac{1}{2\pi j}\int_{-\infty}^{\infty}\frac{(G(t)-G(\eta))H_{az}(t)}{t-\eta}dt = \frac{1}{(2\pi j)^2}\int_{-\infty}^{\infty}M_e(\eta,\eta')H_{oz}(\eta')d\eta' + s_2(\eta) \tag{109}$$

with

$$s_1(\eta) = G(\eta)H_{oz}^{ns}(\eta),\quad s_2(\eta) = \frac{1}{2\pi j}\int_{\gamma_{1t}}\frac{H_{oz}^{ns}(-m(t))}{t-\eta}dt. \tag{110}$$

Let us focus our attention on the source term (110); for simplicity, we assume that only $F_+(\eta) = H_{oz}(\eta)$ is nonstandard:

$$F_+^{ns}(\eta) = H_{oz}^{ns}(\eta) = \frac{2jH_o}{\eta-\eta_o} \tag{111}$$

where $\eta_o = -k\cos(\varphi_o)$, $0 < \varphi_o < \pi/2$ and k has small losses ($k = k_r - jk_i$, $k_i << k_r$). From (111), according to the properties of $-m(\eta)$ (see also Figure 4), $H_{oz}^{ns}(-m(\eta))$ in the proper lower half of the complex η plane shows poles originating from the zeros of $m(\eta) + \eta_o$ (in the m plane, we have the pole $m_o = -\eta_o$). The poles can be related to GO waves, i.e., connected to the last couple of reflections from faces a and o that create shadow boundaries (for instance, see [40]). As an example, if $\varphi_o < \pi - \gamma$, then we have one reflection from face a and one reflection from face o reflected again by face a. In fact, from a mathematical point of view, in this case we have pole m_o related to poles $\eta_{ra} = -k\cos(\gamma - \varphi_o)$ (reflection from face a) and $\eta_{raro} = -k\cos(\gamma + \varphi_o)$ (reflection from a after o), which are associated with incoming azimuthal directions $\gamma \mp \varphi_o$ with respect to the reference face a, i.e., the incoming directions $2\gamma \mp \varphi_o$ with respect to face o. However, we also need to note that the residues of the poles in the selected test problems are always related only to the incident field. This means that the primary spectra of $H_{oz}^{ns}(-m(\eta))$ in (110) are more similar to a replica of the incident spectrum for η_{ra}, η_{raro}, similar to what was described in the w plane in [13].

Indeed, the integrand of the source term in (110) also exhibits a branch cut of $-m(\eta)$. Thus, we estimate (110) by warping γ_{1t} into λ_1, as follows:

$$s_2(\eta) = \frac{1}{2\pi j}\int\limits_{\lambda_1} \frac{H_{oz}^{ns}(-m(t))}{t-\eta}dt + \frac{R_a}{\eta-\eta_{ra}} + \frac{R_{ao}}{\eta-\eta_{raro}} \tag{112}$$

where R_a and R_o are the residues of $H_{oz}(-m(\eta))$ in η_{ra} and η_{raro}, respectively.

$$H_{oz}^{ns}(-m(\eta)) = -\frac{2jH_o}{m(-\eta)+\eta_o} = \frac{T_{m_o}}{m(-\eta)+\eta_o},\ T_{m_o} = -2jH_o \tag{113}$$

$$R_{a,ao} = T_{m_o}\frac{d\eta}{dm}\bigg|_{\eta_{ra},\eta_{raro}} = \frac{2jH_o}{\cos\gamma + \frac{\eta\sin\gamma}{\sqrt{k^2-\eta^2}}}\bigg|_{\eta_{ra},\eta_{raro}} \tag{114}$$

Using the same mathematical procedure that yields (102)–(104) from (101), from (112) we obtain

$$\frac{1}{2\pi j}\int\limits_{\lambda_1} \frac{H_{oz}^{ns}(-m(t))}{t-\eta}dt = \frac{H_o}{\pi}\int_{\lambda_1}\frac{1}{(t-\eta)(-m(t)-\eta_o)}dt = -\frac{H_o}{\pi}M_e(\eta,\eta_o). \tag{115}$$

Thus,

$$s_2(\eta) = -\frac{H_o}{\pi}M_e(\eta,\eta_o) + \frac{R_a}{\eta-\eta_{ra}} + \frac{R_{ao}}{\eta-\eta_{raro}}. \tag{116}$$

The final set of FIEs for H_z polarization when the structure is illuminated by a plane wave with $0 < \varphi_o < \pi/2$ is then (108)–(109) (a specialization of (99)–(100)), with sources $s_{1,2}(\eta)$ being defined and calculated in (110), (111), and (116). Note that $s_1(\eta)$ and $s_2(\eta)$ are spectral components defined in the η plane of $H_{oz}(\eta)$ and $H_{az}(\eta)$, respectively, i.e., with the reference coordinate system of face o and face a.

We now examine the convergence properties of the FIEs in (108)–(109) to obtain accurate numerical results [41]. According to the classical Fredholm factorization method [11], the regularization procedure provides compact kernels of the type reported on the LHS of (108)–(109), i.e., it is square-integrable. The further integral operator reported on the RHS of (108)–(109) in terms of $M_e(\eta,\eta')$ is related to the coupling term between the spectra of delimiting faces. This kernel is again compact, as (101) shows that $M_e(\eta,\eta')$ is never singular for $\eta \neq t$ and $\eta' \neq m(t)$ and (104) shows that $M_e(\eta,\eta')$ is square-integrable according to its asymptotic behavior in terms of (106). Similar considerations can be repeated in more complex and general cases of angular regions immersed in/made of arbitrary linear media.

5.3. Implementation of a Numerical Example and Validation of Direct Fredholm Factorization

Let us consider region 1 in Figure 1 with an aperture angle $\pi/2 < \gamma < \pi$, which is filled by a homogeneous isotropic medium with a propagation constant k ($k = k_r - jk_i$, $k_i << k_r$) and terminated by PEC boundary conditions. The angular region is illuminated by an H_z polarized plane wave with an incoming direction φ_o ($0 < \varphi_o < \pi - \gamma$) and intensity H_o. The spectral solution $(H_{oz}(\eta), H_{az}(\eta))$ can be provided by the system of FIEs in (108)–(109). Due to the convergence properties of the kernel [41], simple sample-and-hold approximation is enforced with the truncation of integration intervals at $\pm A$ and integration step h such that $A/h \in \mathbb{N}$. We tested our novel direct FIE solution against the classical exact closed-form solution provided in Section 5.1 in the η and w planes, respectively ((88) and (89)). Furthermore, we compared the asymptotic results in terms of GTD coefficients. We examine the case where $\gamma = 0.7\pi$, $k = 1 - j0.1$, $H_o = 1A/m$, and $\varphi_o = 0.1\pi$ in detail. Because we have $0 < \varphi_o < \pi - \gamma$, the GO field is constituted by the incident waves, waves reflected by face a, and doubly-reflected waves (from face o and then from face a); only the plus spectral unknown along face o, i.e., $H_{oz}(\eta)$, is nonstandard

in the WH formulation (91), as reported in the example in the previous subsection. To enhance the convergence of the approximate FIE solution provided by (108)–(109), we warp the integration line constituted by the real axis into a straight line located in the first and third quadrants of the complex plane at an angle θ with respect to the real axis (the singularities of the kernel and the sources are located in the second and fourth quadrants; see Sections 5.3 and 5.4 of [12]):

$$\alpha_t(t) = t\exp^{j\theta},\ t \in \mathbb{R},\ 0 < \theta < \pi/2. \tag{117}$$

According to the physical parameters of the test problem, we have $\eta_{ra} = 0.309017 - 0.0309017j$, $\eta_{raro} = 0.809017 - 0.0809017j$, with both located in the lower half-plane, as considered in (116). The discretization of (108)–(109) by the sample-and-hold technique with A, h yields a linear system of equations with dimensions of $2(2(A/h)+1)$:

$$\left|\begin{array}{cc} \underline{\underline{d}}_G + \underline{\underline{K}}_G & -\underline{\underline{M}}_e \\ -\underline{\underline{M}}_e & \underline{\underline{d}}_G + \underline{\underline{K}}_G \end{array}\right| \left|\begin{array}{c} \underline{H}_{oz} \\ \underline{H}_{az} \end{array}\right| = \left|\begin{array}{c} \underline{s}_1 \\ \underline{s}_2 \end{array}\right| \tag{118}$$

where the diagonal matrix $\underline{\underline{d}}_G$, the matrix $\underline{\underline{K}}_G$, and the matrix $\underline{\underline{M}}_e$ contain samples of $G(\eta)$, $\frac{G(t)-G(\eta)}{t-\eta}$, and $M_e(\eta,\eta')$, respectively, while the vectors $\underline{H}_{oz}$, $\underline{H}_{az}$ and $\underline{s}_1$, $\underline{s}_2$ contain samples of $H_{oz}(\eta)$, $H_{az}(\eta)$ and $s_1(\eta)$, $s_2(\eta)$, respectively. Note that $\underline{\underline{M}}_e$ is a coupling matrix that is much weaker than the remaining terms. The sampled solutions allow for a representation of $H_{oz}(\eta)$, $H_{az}(\eta)$ to be built by substituting them into the integral part of (108)–(109):

$$H_{oz,az}(\eta) = -\frac{h}{2\pi j}\sum_{-A/h}^{A/h}\frac{[G^{-1}(\eta)G(\alpha_t(hi))-1]H_{oz,az}(\alpha_t(hi))}{\alpha_t(hi)-\eta} + \frac{hG^{-1}(\eta)}{(2\pi j)^2}\sum_{-A/h}^{A/h} M_e(\eta,\alpha_t(hi))H_{az,oz}(\alpha_t(hi)) + G^{-1}(\eta)s_{1,2}(\eta). \tag{119}$$

These approximate expressions of $H_{oz}(\eta)$, $H_{az}(\eta)$ are valid for analytic continuation in the proper sheet of the η plane, which is useful for correctly estimating fields in the physical domain through the asymptotics of half-planes, as discussed in Section 4. This property limits the requirement to know the spectra only in the proper sheet, as acquired in the procedure, which is a novelty and represents progress with respect to classical Fredholm factorization combined with spectral mapping in GWHE wedge problems.

To highlight the performance of this method, we compare the spectra along the real axis of the η plane and a segment of the η plane that is useful for asymptotics according to the steepest descent path (SDP) method, which in an isotropic medium corresponds to $\eta = -k\cos w$ with $-\pi < w < 0$, i.e., the segment that connects $-k$ with k.

To study the convergence of the method, we select physical parameters of region 1 with an aperture angle of $\gamma = 0.7\pi$ and plane wave illumination at H_z polarization with $H_o = 1A/m$, $\varphi_o = 0.1\pi$, and $k = 1 - j0.1$. We select the quadrature parameters $5 \leq A \leq 40$, $0.2 \leq h \leq 0.25$, $\theta = 0.1$ such that $A/h \in \mathbb{N}$. The numerical results are provided in Figure 6 along the segment for asymptotic estimation. In the figure, we note that along the segment we have a degradation of the spectral solution near $w = -\pi, 0$, which corresponds to the branch points $\eta = k, -k$ of ξ (where ξ defines the proper and improper sheet of the η plane [11]). We recall that the solution of the FIEs was obtained through the simple sample-and-hold quadrature and estimation of $M_e(\eta,\eta')$, which saturates the precision, particularly near $\eta = k, -k$ (the branch point $\eta = -k$ is a local offending singularity for the plus spectra that should not appear, while $\eta = k$ is related to physical structural properties of the problem). An improvement would be obtained with a specialized quadrature (and method of moments) capable of taking into account non-algebraic behavior such as branch points (see [42]); however, the scope of the present method involves obtaining a very simple, fast, and convergent solution that cannot incorporate sophisticated quadratures. Furthermore, we observe that the lack of precision near $\eta = k, -k$ is mitigated while computing asymptotics because plus spectral unknowns are multiplied by $\sin w$, providing locally-smoothing errors. However, while the offending $\eta = -k$ is a very local perturbation, the physical $\eta = k$ is more present, as it is physical.

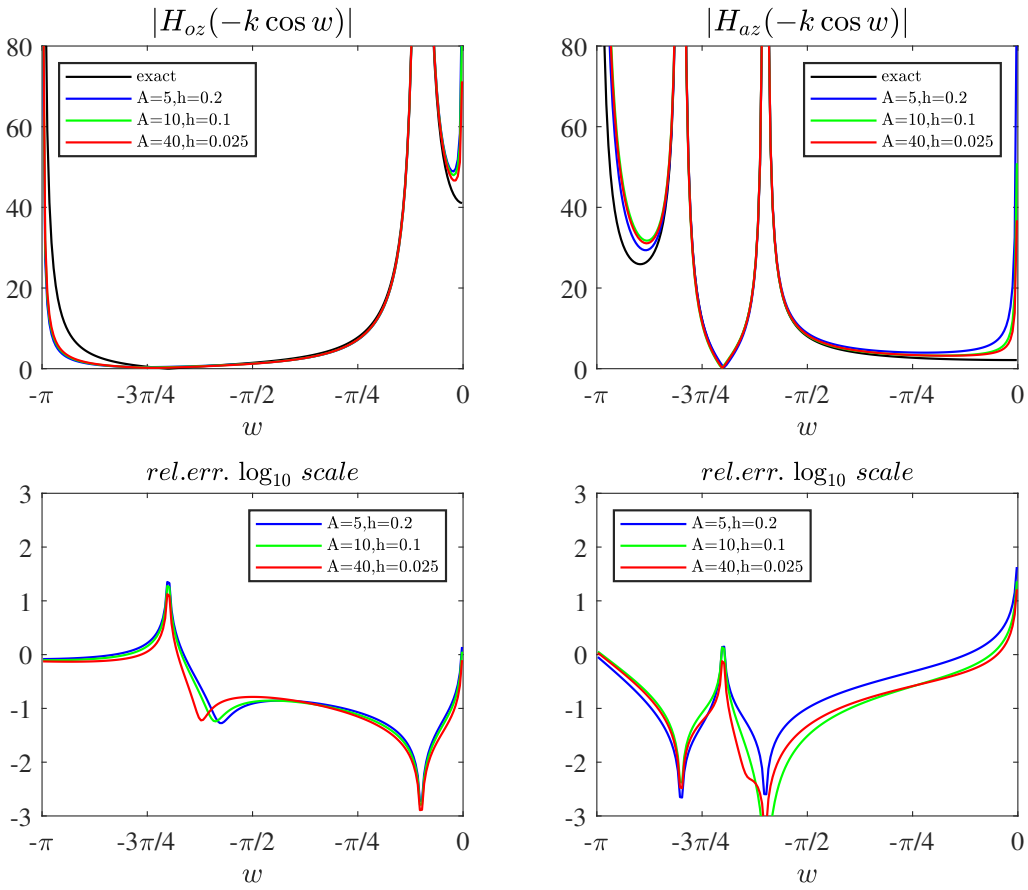

Figure 6. On top, plots of the absolute values of the spectral solutions $|H_{oz}(-k\cos w)|$ and $|H_{az}(-k\cos w)|$ obtained as exact solutions and with the FIE approximations for different values of A, h. On the bottom, the corresponding relative errors between the exact solutions and the FIE solutions for different values of A, h on a $\log_{10}$ scale. Degradation of the spectral solution can be observed near $w = -\pi, 0$, which corresponds to $\eta = k, -k$. The branch point $\eta = -k$ is an offending singularity for the plus spectra, while $\eta = k$ is related to the physical structural properties of the problem.

To recover the quality of the solution near $w = -\pi, 0$ ($\eta = k, -k$), we resort to spectral considerations based on the properties of the original GWHE formulation in (91). Equation (91) can be applied to the approximate solutions obtained from the FIEs to obtain a new improved representation of the plus spectra. This application allows us to obtain an approximate spectrum near $w = -\pi, 0$ ($\eta = k, -k$) that originates from another portion of the η plane according to $m(\eta)$. This procedure is particularly effective and valid because $m(\eta)$ for η in the proper sheet lies in just a portion of the proper sheet of the η plane. This property is particularly evident (in this simplified isotropic problem) by rewriting (91) in the w plane:

$$\begin{aligned} H_{oz}(-k\cos w) &= \frac{-n(-k\cos w)}{\xi(-k\cos w)} H_{az}(-k\cos(w+\gamma)) \\ H_{az}(-k\cos w) &= \frac{-n(-k\cos w)}{\xi(-k\cos w)} H_{oz}(-k\cos(w+\gamma)) \end{aligned} \tag{120}$$

with $\xi(-k\cos w) = -k\sin w$ and $-n = -k\sin(w+\gamma)$. We note that $-\pi < w < 0$ on the LHS corresponds to $-\pi + \gamma < w < \gamma$ on the RHS due to $(m = k\cos(w+\gamma))$, where the unknowns are correctly computed. This methodology (named iteration) reimposes GWHEs on the initial FIE-approximated spectra and shifts the lack of precision to a region where the spectral solution is good, yielding a homogenization of the error level (see Figure 7). In the figure, we report (1) the exact solution, (2) the approximate solution obtained from the quadrature of FIEs with $A = 40, h = 0.025$, (3) the approximate solution obtained from the quadrature of FIEs with $A = 40, h = 0.025$ plus the application of (91), and (4) the

approximate solution obtained from the application of (91) to the sources of FIEs while ignoring integral terms, i.e., using $H_{oz,az}(\eta) = +G^{-1}(\eta)s_{1,2}(\eta)$.

Note that when considering (91), the map in (120) is only limited; thus, we cannot interpret this procedure as a first iteration of the application of the contraction theorem. In fact, according to our studies, successive iterations do not yield any benefit in the convergence of the solution. This is also justified by the fact that in the w plane, the multiple applications of (120) correspond to recursive equations/difference equations that further shift the spectra in the w plane, thereby navigating replicas of the proper and improper sheets of the η plane defined by ξ; see [11,13]. Moreover, the map is also excluded from compensating for all physical behaviors of the problem starting from roughly approximate solutions. Figure 7 shows the importance of the quality of starting spectra that originate from the solution of the FIEs before the application of (120).

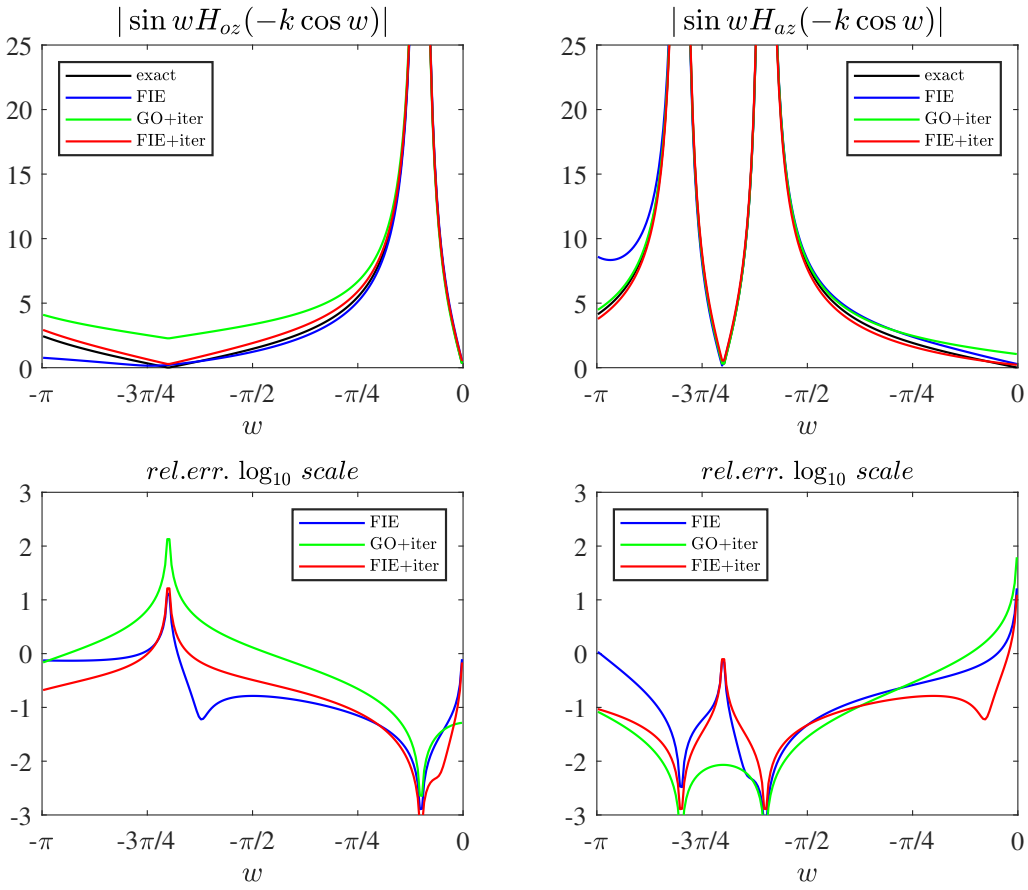

Figure 7. On top, plots of the absolute values of the spectral solutions $|\sin w\, H_{oz}(-k\cos w)|$ and $|\sin w\, H_{az}(-k\cos w)|$ obtained as exact solutions and with (1) the FIEs with $A = 40, h = 0.025$, (2) the FIEs plus application of one iteration of (91) (FIE+iter), and (3) application of (91) to the source terms of the FIEs (GO+iter). On the bottom, the corresponding relative errors between the exact solutions and the approximate solutions. It is possible to observe an improvement of the solutions near $w = -\pi, 0$ after applying an iteration of (91) to the approximate solution from the FIEs, yielding a homogenization of the error.

Finally, we observe that while the FIEs provide good spectra except near the branch cuts, the iteration in (91) enforces correct modeling of structural spectral properties such as branch cuts.

To further compare the solutions and validate the proposed procedure, we have computed the GTD diffraction coefficient as outlined in Section 4 using asymptoptics. Using superposition, we can compute the diffraction by applying asymptotics individually to the spectral solutions at faces o and a while considering only homogeneous terms

in (56) and (59). This takes care of the different reference coordinates (see the discussion in Sections 3 and 4 considering region 1 characterized by γ as region 2′ characterized by $\pi - \gamma$; see Figures 1 and 2, (45), and (59)):

$$\tilde{\boldsymbol{\psi}}_{\boldsymbol{y}}^{\boldsymbol{ho}}(\eta, v) = \sum_{i=1}^{2} \boldsymbol{v_i} \cdot \tilde{\boldsymbol{\psi}}_{\boldsymbol{y}}(\eta, 0) e^{-\lambda_{\gamma i}(\gamma)\, v} \boldsymbol{u_i},\ v > 0, \tag{121}$$

$$\tilde{\boldsymbol{\psi}}_{\boldsymbol{Y1}}^{\boldsymbol{ho}}(\eta, v) = \sum_{i=3}^{4} \boldsymbol{v_{iY_1}} \cdot \tilde{\boldsymbol{\psi}}_{\boldsymbol{Y1}}(\eta, 0) e^{-\lambda_{\gamma i Y_1}(\pi-\gamma)\, v} \boldsymbol{u_{iY_1}},\ v < 0. \tag{122}$$

Starting from the inversion of the contribution of face o (121), we have

$$\boldsymbol{\psi}_{\boldsymbol{y}}^{\boldsymbol{ho}}(u, v) = \frac{1}{2\pi} \int_{B_r} \tilde{\boldsymbol{\psi}}_{\boldsymbol{y}}^{\boldsymbol{ho}}(\eta, v) e^{-j\eta u} d\eta. \tag{123}$$

According to the coordinate mapping in (18), from (16) and (23) we have

$$-\lambda_{\gamma i}(\gamma)\, v - j\eta u = -j\eta \cos\gamma\, v - j\xi_i \sin\gamma v - j\eta(x - v\cos\gamma) = -j(\eta x + \xi_i y),\ i = 1, 2 \tag{124}$$

with $\xi_i = \xi$, $i = 1, 2$; thus,

$$\boldsymbol{\psi}_{\boldsymbol{y}}^{\boldsymbol{ho}}(x, y) = \frac{1}{2\pi} \int_{B_r} \sum_{i=1}^{2} \boldsymbol{v_i} \cdot \tilde{\boldsymbol{\psi}}_{\boldsymbol{y}}(\eta, 0) \boldsymbol{u_i} e^{-j(\eta x + \xi y)} d\eta, \tag{125}$$

where B_r is the Bromwich contour (over all singularities). The asymptotic estimation of (125) at the far field is composed of GO terms (captured poles) and GTD diffracted components (due to the saddle point with the application of the SDP method); in global cylindrical coordinates, this is

$$\boldsymbol{\psi}_{\boldsymbol{y}}^{\boldsymbol{ho,gtd}}(\rho, \varphi) = \sqrt{\frac{k}{2\pi\rho}} e^{-j(k\rho - \pi/4)} \sum_{i=1}^{2} \boldsymbol{v_i} \cdot \tilde{\boldsymbol{\psi}}_{\boldsymbol{y}}(k\cos\varphi, 0) \boldsymbol{u_i} \sin|\varphi|. \tag{126}$$

In our test problem (region 1 with PEC faces with H_z polarization), this reduces to the third component

$$\boldsymbol{\psi}_{\boldsymbol{y}}^{\boldsymbol{ho,gtd}}(\rho, \varphi)[3] = H_{oz}^{gtd}(\rho, \varphi) = \sqrt{\frac{k}{2\pi\rho}} e^{-j(k\rho - \pi/4)} \frac{H_{oz}(k\cos\varphi)}{2} \sin|\varphi| \tag{127}$$

according to the definition of $\tilde{\boldsymbol{\psi}}_{\boldsymbol{y}}(\eta, v)$ in (3) and $\boldsymbol{u_i}, \boldsymbol{v_i}$ in (62)–(63). We obtain the following GTD diffraction coefficient component due to face o:

$$D_{Hoz}^{gtd}(\varphi) = \frac{kH_{oz}(k\cos\varphi)\sin|\varphi|}{j2H_o}. \tag{128}$$

Now, we repeat the procedure starting from the inversion of the contribution of face a (122) using the notation in Figures 1 and 2b:

$$\boldsymbol{\psi}_{\boldsymbol{Y1}}^{\boldsymbol{ho}}(u, v) = \frac{1}{2\pi} \int_{B_r} \tilde{\boldsymbol{\psi}}_{\boldsymbol{Y1}}^{\boldsymbol{ho}}(\eta, v) e^{-j\eta u} d\eta. \tag{129}$$

According to the coordinate mapping

$$X_1 = u + v\cos(\pi - \gamma),\ Y_1 = v\sin(\pi - \gamma), \tag{130}$$

from (16) and (23) we have

$$-\lambda_{\gamma i Y_1}(\pi - \gamma)\, v - j\eta u = +j\eta\cos\gamma\, v + j\xi_i \sin\gamma v - j\eta(X_1 + v\cos\gamma) = -j\eta X_1 + j\xi_i Y_1,\ i = 3, 4 \tag{131}$$

where $\xi_i = \xi$, $i = 3, 4$; thus,

$$\boldsymbol{\psi}_{\mathbf{Y1}}^{\boldsymbol{ho}}(X_1, Y_1) = \frac{1}{2\pi} \int_{B_r} \sum_{i=3}^{4} \boldsymbol{v}_{i\mathbf{Y}_1} \cdot \tilde{\boldsymbol{\psi}}_{\mathbf{Y1}}(\eta, 0) \boldsymbol{u}_{i\mathbf{Y}_1} e^{-j\eta X_1 + j\xi Y_1} d\eta, \tag{132}$$

where B_r is a Bromwich contour. The asymptotic estimation of (132) at the far field is composed of GO terms and GTD diffracted components in the following global cylindrical coordinates:

$$\boldsymbol{\psi}_{\mathbf{Y1}}^{\boldsymbol{ho,gtd}}(\rho, \varphi) = \sqrt{\frac{k}{2\pi\rho}} e^{-j(k\rho - \pi/4)} \sum_{i=3}^{4} \boldsymbol{v}_{i\mathbf{Y}_1} \cdot \tilde{\boldsymbol{\psi}}_{\mathbf{Y1}}(k\cos(\varphi - \gamma), 0) \boldsymbol{u}_{i\mathbf{Y}_1} \sin|\varphi - \gamma|. \tag{133}$$

For our test problem (region 1 with PEC faces with H_z polarization), this reduces to the third component

$$\boldsymbol{\psi}_{\mathbf{Y1}}^{\boldsymbol{ho,gtd}}(\rho, \varphi)[3] = H_{az}^{gtd}(\rho, \varphi) = \sqrt{\frac{k}{2\pi\rho}} e^{-j(k\rho - \pi/4)} \frac{H_{az}(k\cos(\varphi - \gamma))}{2} \sin|\varphi - \gamma| \tag{134}$$

according to the definition of $\tilde{\boldsymbol{\psi}}_{\boldsymbol{y}}(\eta, v)$ in (3) and $\boldsymbol{u}_{i\mathbf{Y}_1} = \boldsymbol{u}_i, \boldsymbol{v}_{i\mathbf{Y}_1} = \boldsymbol{v}_i$ in (62)–(63). Note that the invariance of $\boldsymbol{u}_{i\mathbf{Y}_1} = \boldsymbol{u}_i, \boldsymbol{v}_{i\mathbf{Y}_1} = \boldsymbol{v}_i$ in the rotation of the reference system is allowable only in isotropic regions; otherwise, a more complex procedure is required for their definition in arbitrary linear media (see Section 2).

Finally, we obtain the following GTD diffraction coefficient component due to face a:

$$D_{Haz}^{gtd}(\varphi) = \frac{kH_{az}(k\cos(\varphi - \gamma))\sin|\varphi - \gamma|}{j2H_o}. \tag{135}$$

The complete GTD coefficient is just the sum for the superposition of (128) and (135):

$$D_{Hz}^{gtd}(\varphi) = D_{Hoz}^{gtd}(\varphi) + D_{Haz}^{gtd}(\varphi). \tag{136}$$

Figure 8 shows the GTD diffraction coefficient for the test problem under consideration, that is, $\gamma = 0.7\pi$ and plane wave illumination with H_z polarization with $H_o = 1A/m$, $\varphi_o = 0.1\pi$, and $k = 1 - j0.1$. The figure reports the exact GTD coefficient in terms of the absolute value and phase together with those obtained with the FIE-approximated estimation of the spectra without and with the application of an iteration while selecting $A = 20, h = 0.05, \theta = 0.1$. Figure 9 shows the corresponding relative error of the GTD diffraction coefficient on a $\log_{10}$ scale.

We note, as expected, that the solution with the iteration is correct, while the solution without the iteration is lacking in its estimation near the faces of the angular regions, i.e., face o for $\varphi = 0$ and face a for $\varphi = \gamma$, as they are related to the spectra of $H_{oz}(\eta)$ near $\eta = k$ (128) and $H_{az}(\eta)$ near $\eta = k$ (135), respectively ($\eta = k$ corresponds to $w = -\pi$, and is a physical branch point). In addition, note that the spectra of $H_{oz}(\eta), H_{az}(\eta)$ near $\eta = -k$ ($w = 0$) are not used for the GTD computation; thus, the lack of possible precision in the offending branch point does not impact the quality of the solution. Moreover, the change in the slope and level of the relative error in Figure 9 is obtained using the reported algorithm to improve the quality of the approximate solution provided by the direct application of Fredholm factorization. In fact, FIE+iteration involves computation of the GTD diffraction coefficient in (136) via (128) and (135), where the spectra $H_{oz}(-k\cos w)$ and $H_{az}(-k\cos w)$ are obtained by enforcing (120) on the approximate spectra obtained through the direct application of Fredholm factorization. This procedure mixes the spectral resolution properties of the two faces, thereby improving the quality of the spectra and recovering the degradation of the spectral resolution near $w = \pi, 0$, i.e., $\eta = k, -k$.

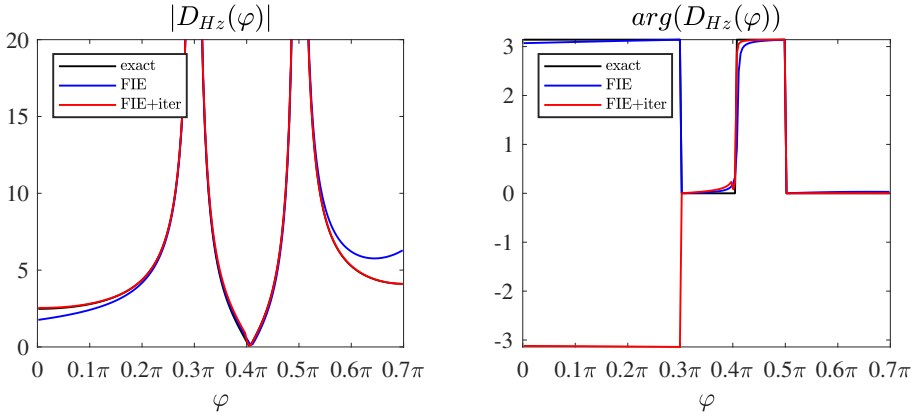

Figure 8. GTD diffraction coefficient (absolute value and phase) for the test problem under consideration: $\gamma = 0.7\pi$ and plane wave illumination with H_z polarization with $H_o = 1A/m$, $\varphi_o = 0.1\pi$, and $k = 1 - j0.1$. The figure reports the exact GTD coefficient together with those obtained with the FIE-approximated estimation of the spectra without and with the application of an iteration while selecting $A = 20, h = 0.05, \theta = 0.1$.

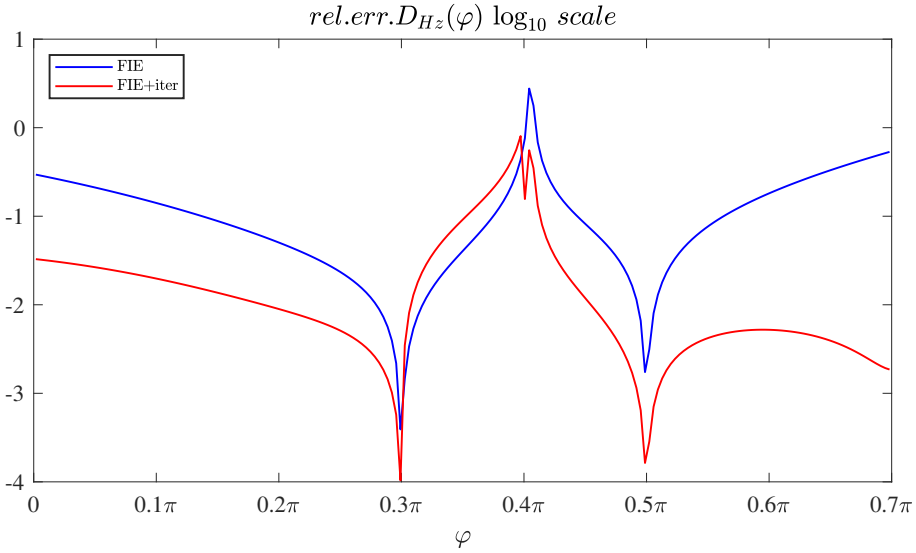

Figure 9. Relative error of the GTD diffraction coefficient on a $\log_{10}$ scale corresponding to the results in Figure 8.

Finally, we comment that the direct implementation of FIEs in the w plane yields high-precision results in isotropic angular region problems [12], exceeding the precision of the current procedure in terms of spectra; however, we recall that the scope of the present work involves presenting an effective procedure for computing diffraction that is implementable in problems where the w plane cannot be defined, such as in arbitrarily linear media.

6. An Example of the Application of the Functional Equations in Complex Media: Scattering from a PEC Half-Plane in a Gyrotropic Medium

The scattering of an electromagnetic plane wave at normal incidence by a perfectly conducting semi-infinite screen embedded in a homogeneous gyrotropic medium (such as plasma) is presented in this section with the goal of validating the proposed method, the functional equations, and the WH equations in nonisotropic media. As our formulation is in terms of field components, we selected [15,16,20,21] as studies for comparison; we did not consider other literature where definitions in terms of potentials were employed. In particular, we selected [15], where the distinguished axis of the electric gyrotropic medium is parallel to the edge of the half-plane, i.e., as in plasma, with a uniform magnetic field

impressed along the edge direction. This medium enforces a tensorial electric permittivity, which in our reference system of coordinates (z, x, y) is

$$\underline{\underline{\boldsymbol{\varepsilon}}} = \begin{bmatrix} \varepsilon_3 & 0 & 0 \\ 0 & \varepsilon_1 & +j\varepsilon_2 \\ 0 & -j\varepsilon_2 & \varepsilon_1 \end{bmatrix}, \tag{137}$$

where z is the distinguished axis of the medium and $\underline{\underline{\boldsymbol{\mu}}} = \mu_o \underline{\underline{\boldsymbol{I}}}$, $\underline{\underline{\boldsymbol{\xi}}} = \underline{\underline{\boldsymbol{\zeta}}} = \underline{\underline{\boldsymbol{0}}}$. As reported in [15], this vector problem is separable into two equivalent scalar problems for the E_z (H-mode) and H_z (E-mode) polarizations.

By applying the procedure described in Section 2 and with simplified definitions of the quantities reported in Appendix A, we obtain the following (progressive, regressive) eigenvalues:

$$\lambda_{1,3} = \pm\sqrt{\eta^2 - k_1^2} = \pm j\xi_1, \quad \lambda_{2,4} = \pm\sqrt{\eta^2 - k_2^2} = \pm j\xi_2 \tag{138}$$

where $k_1^2 = \omega^2\mu_o\varepsilon/\varepsilon_1 = k_o^2\varepsilon/\varepsilon_1$, $k_2^2 = \omega^2\mu_o\varepsilon_3 = k_o^2\varepsilon_{r3}$, $\varepsilon_{ri} = \varepsilon_i/\varepsilon_o$, $\varepsilon = \varepsilon_1^2 - \varepsilon_2^2$, and $k_o = \omega\sqrt{\varepsilon_o\mu_o}$.

The corresponding eigenvectors $\boldsymbol{u_i}$, from which we can easily compute the reciprocal vectors $\boldsymbol{v_i}$ through inversion, are

$$\boldsymbol{u_1} = \begin{vmatrix} 0 \\ \frac{j(-\varepsilon_2\eta + \varepsilon_1 j\xi_1)}{\varepsilon\omega} \\ 1 \\ 0 \end{vmatrix}, \ \boldsymbol{u_2} = \begin{vmatrix} \frac{\mu_o\omega}{\varepsilon_2} \\ 0 \\ 0 \\ 1 \end{vmatrix}, \ \boldsymbol{u_3} = \begin{vmatrix} 0 \\ -\frac{j(\varepsilon_2\eta + \varepsilon_1 j\xi_1)}{\varepsilon\omega} \\ 1 \\ 0 \end{vmatrix}, \ \boldsymbol{u_4} = \begin{vmatrix} -\frac{\mu_o\omega}{\varepsilon_2} \\ 0 \\ 0 \\ 1 \end{vmatrix}. \tag{139}$$

The problem shows simplification because of $\gamma = \pi$; see for instance the impact of the anisotropies on (35) or

$$m = m_i(\pi - \gamma) = m_{i+2}(\gamma) = \eta; \quad i = 1, 2. \tag{140}$$

However, we keep the procedure as general as possible, i.e., applicable to wedge problems (arbitrary γ); from (27) and (31), we obtain

$$\tilde{\boldsymbol{\psi}}_{\boldsymbol{sa}+}(-m_i(\gamma)) = \left| \ E_{az}\cos(\gamma), E_{a\rho} + \frac{\eta H_{az}\sin(\gamma)}{\omega\varepsilon_1}, H_{az}\cos(\gamma) - \frac{jH_{az}\varepsilon_2\sin(\gamma)}{\varepsilon_1}, H_{a\rho} - \frac{E_{az}\eta\sin(\gamma)}{\mu_o\omega} \ \right|^t. \tag{141}$$

From here on, we omit the spectral dependence in the field components for better compactness of the formulae. Applying (32), we obtain the following two functional equations for region 1 in explicit form:

$$E_{ox}\omega\varepsilon + H_{oz}\xi_1\varepsilon_1 + j\eta H_{oz}\varepsilon_2 = H_{az}[\sin(\gamma)(\eta\varepsilon_1 - j\xi_1\varepsilon_2) + \cos(\gamma)(\xi_1\varepsilon_1 + j\eta\varepsilon_2)] + E_{a\rho}\varepsilon\omega, \tag{142}$$

$$H_{ox}\mu_o\omega - E_{oz}\xi_2 = H_{a\rho}\mu_o\omega. \tag{143}$$

Similarly, the procedure can be repeated for region 2. The complete set of equations highlights the decoupling of E_z from H_z polarization. Applying the PEC boundary conditions on the faces, after some manipulations we obtain the following equations for the E_z and H_z polarizations:

$$\begin{cases} H_{ox} = \frac{H_{a\rho}}{2} + \frac{H_{b\rho}}{2} \\ -\frac{E_{oz}\xi_2}{\mu_o\omega} = \frac{H_{a\rho}}{2} - \frac{H_{b\rho}}{2} \end{cases} \tag{144}$$

$$\begin{cases} E_{ox}\omega\varepsilon + H_{oz}\xi_1\varepsilon_1 + j\eta H_{oz}\varepsilon_2 = H_{az}[\sin(\gamma)(\eta\varepsilon_1 - j\xi_1\varepsilon_2) + \cos(\gamma)(\xi_1\varepsilon_1 + j\eta\varepsilon_2)] \\ -E_{ox}\omega\varepsilon + H_{oz}\xi_1\varepsilon_1 - j\eta H_{oz}\varepsilon_2 = H_{bz}[\sin(\gamma)(\eta\varepsilon_1 + j\xi_1\varepsilon_2) + \cos(\gamma)(\xi_1\varepsilon_1 - j\eta\varepsilon_2)]. \end{cases} \tag{145}$$

Now, we impose $\gamma = \pi$, i.e., the angular regions are defined for the half-plane problem. In (144), we note that E_z polarization behaves as a half-plane problem immersed in a classical

isotropic region [33] but with a propagation constant of $k_2^2 = \omega^2\mu_o\varepsilon_3 = k_o^2\varepsilon_{r3}$, i.e., this can be interpreted via a network representation with characteristic impedance $Z_{Ez} = \omega\mu_o/\xi_2$, confirming the findings of [15].

With further mathematical manipulation of (145), we obtain

$$\begin{cases} -2H_{oz} + \frac{2iE_{ox}\eta\omega\varepsilon\varepsilon_2}{\xi_1^2\varepsilon_1^2+\eta^2\varepsilon_2^2} = H_{az} + H_{bz} \\ -\frac{2E_{ox}\xi_1\omega\varepsilon\varepsilon_1}{\xi_1^2\varepsilon_1^2+\eta^2\varepsilon_2^2} = H_{az} - H_{bz} \end{cases} \tag{146}$$

and the second equation in (146) shows the same WH kernel as that of Equation (25) in [15]:

$$G_{H_z}^{-1} = -\frac{\xi_1^2\varepsilon_1^2 + \eta^2\varepsilon_2^2}{2\xi_1\omega\varepsilon\varepsilon_1} = -\frac{(k_1^2-\eta^2)\varepsilon_1^2 + \eta^2\varepsilon_2^2}{2\sqrt{k_1^2-\eta^2}\omega\varepsilon\varepsilon_1} = -\frac{k_1^2\varepsilon_1^2/\varepsilon - \eta^2}{2\sqrt{k_1^2-\eta^2}\omega\varepsilon_1} \tag{147}$$

with the sole irrelevant distinction of a multiplication by a scalar. Moreover, the characteristic pole of the surface wave phenomenon is easily recognizable from the numerator, as also found in [15]. The solutions to the problem can be achieved with the proposed approximate technique that was validated in previous sections or via the classical WH procedure, as in [15]; however, this is beyond the scope of the present study.

7. Conclusions

Spectral methods (such as SM, KL, and WH) are well-consolidated, fundamental, and effective tools for the correct and precise analysis of electromagnetic diffraction problems with one propagation constant, although they are not immediately applicable to problems with multiple propagation constants.

In this study, we propose a comprehensive theoretical package in the spectral domain with all necessary mathematical tools that for the first time extends the possibilities of spectral analysis to electromagnetic problems involving wedges immersed in an arbitrary linear medium, and is additionally extendable to multiple penetrable angular regions. The theory is presented in an exhaustive way, showing the theoretical background, implementation, and validation. The methodology is based on transverse equations for layered angular structures, the characteristic Green function procedure, the Wiener–Hopf technique, and our novel direct Fredholm factorization method, which reduces GWHEs with multiple propagation constants to integral representations in a unique complex plane. Validation through examples is applied, starting from demonstrating the effectiveness of direct Fredholm factorization applied to GWHEs in the scattering from a PEC wedge immersed in an isotropic medium and ending with the validation of functional equations of angular regions in arbitrary linear media with the analysis of a PEC half-plane immersed in particular anisotropic media. While numerically implementing the method, we observed that one of the main difficulties resides in the correct estimation of kernel functions for the presence of multivalued functions that need particular attention in their definition and calculation.

The proposed equations are interpreted using a network formalism in order to provide a systematic perspective, particularly for the analysis of complex scattering problems where the complexity of the geometry is broken into subdomains of canonical shapes in which the angular regions are immersed in/made of arbitrarily linear media.

This work presents significant advancements in the spectral analysis of electromagnetic problems from different mathematical, physical, and engineering perspectives: (1) the first spectral method capable of handling scattering in arbitrary linear media with multiple propagation constants; (2) direct Fredholm factorization, a novel solution procedure for GWHEs, particularly those with multiple propagation constants; (3) a network interpretation of spectral functional equations and related integral representations for angular regions filled by arbitrary linear media (4) computation of the field at each point within the angular region, avoiding spectral analytical extension; and (5) improved quality of approximate spectral solutions from FIEs by reimposing the GWHEs of the problem, which we name iteration.

This theoretical package has been validated and is ready for future applications.

Author Contributions: V.G.D. and G.L. collaborated in the conceptualization, methodology, mathematics, formal analysis, investigation, validation, writing—original draft preparation, writing—review and editing, project administration, and funding acquisition. All authors have read and agreed to the published version of the manuscript.

Funding: This research was funded by the Italian Ministry of Universities and Research under PRIN Grant 2017NT5W7Z GREEN TAGS and Next-Generation EU-PNRR M4C2-Inv 1.4–National Centre for HPC, Big Data, and Quantum Computing (HPC)—Multiscale Modeling and Engineering App.

Institutional Review Board Statement: Not applicable.

Informed Consent Statement: Not applicable.

Data Availability Statement: The original contributions presented in this study are included in the article and the Appendix A; further inquiries can be directed to the corresponding authors. The data presented in this study were obtained by means of an in-house software code implementing the proposed method.

Conflicts of Interest: The authors declare no conflicts of interest.

Appendix A. Explicit Form of Expressions Used in the Main Text

Appendix A contains details and supplements to the main text, in particular explicit expressions that would be cumbersome to report in the main text due to issues with readability and preserving completeness.

The explicit expressions of the 4×4 matrices $\boldsymbol{M}_{yo}, \boldsymbol{M}_{y1}, \boldsymbol{M}_{y2}$ used in Section 2 for (4), i.e.,

$$\boldsymbol{M}_{\boldsymbol{y}}(-j\alpha_o, \frac{\partial}{\partial x}) = \boldsymbol{M}_{yo} + (\frac{\partial}{\partial x})\boldsymbol{M}_{y1} + (\frac{\partial}{\partial x})^2\boldsymbol{M}_{y2} \tag{A1}$$

for arbitrary linear media are presented in factorized form as follows:

$$\boldsymbol{M}_{yo} = \frac{j(\omega \boldsymbol{M}_{yo}^{(0)} + \alpha_o \boldsymbol{M}_{yo}^{(1)} + \alpha_o^2 \boldsymbol{M}_{yo}^{(2)}/\omega)}{\epsilon_{yy}\mu_{yy} - \zeta_{yy}\xi_{yy}} \tag{A2}$$

$$\boldsymbol{M}_{yo}^{(0)} = \begin{pmatrix} \zeta_{xy}\zeta_{yz}\xi_{yy} - \zeta_{xz}\zeta_{yy}\xi_{yy} + \zeta_{xz}\mu_{yy}\epsilon_{yy} - \zeta_{yz}\mu_{xy}\epsilon_{yy} - \zeta_{xy}\mu_{yy}\epsilon_{yz} + \zeta_{yy}\mu_{xy}\epsilon_{yz} & -\zeta_{xx}\zeta_{yy}\xi_{yy} + \zeta_{xy}\zeta_{yx}\xi_{yy} - \zeta_{xy}\mu_{yy}\epsilon_{yx} + \zeta_{yy}\mu_{xy}\epsilon_{yx} + \zeta_{xx}\mu_{yy}\epsilon_{yy} - \zeta_{yx}\mu_{xy}\epsilon_{yy} \\ \zeta_{yy}\zeta_{zz}\xi_{yy} - \zeta_{yz}\zeta_{zy}\xi_{yy} + \zeta_{yz}\mu_{zy}\epsilon_{yy} - \zeta_{zz}\mu_{yy}\epsilon_{yy} - \zeta_{yy}\mu_{zy}\epsilon_{yz} + \zeta_{zy}\mu_{yy}\epsilon_{yz} & -\zeta_{yx}\zeta_{zy}\xi_{yy} + \zeta_{yy}\zeta_{zx}\xi_{yy} - \zeta_{yy}\mu_{zy}\epsilon_{yx} + \zeta_{zy}\mu_{yy}\epsilon_{yx} + \zeta_{yx}\mu_{zy}\epsilon_{yy} - \zeta_{zx}\mu_{yy}\epsilon_{yy} \\ -\zeta_{yz}\xi_{yy}\epsilon_{xy} + \mu_{yy}\epsilon_{xy}\epsilon_{yz} + \zeta_{yy}\xi_{yy}\epsilon_{xz} - \mu_{yy}\epsilon_{xz}\epsilon_{yy} + \zeta_{yz}\xi_{xy}\epsilon_{yy} - \zeta_{yy}\xi_{xy}\epsilon_{yz} & \zeta_{yy}\xi_{yy}\epsilon_{xx} - \mu_{yy}\epsilon_{xx}\epsilon_{yy} - \zeta_{yx}\xi_{yy}\epsilon_{xy} + \mu_{yy}\epsilon_{xy}\epsilon_{yx} - \zeta_{yy}\xi_{xy}\epsilon_{yx} + \zeta_{yx}\xi_{xy}\epsilon_{yy} \\ -\zeta_{yz}\xi_{zy}\epsilon_{yy} + \mu_{yy}\epsilon_{yy}\epsilon_{zz} + \zeta_{yy}\xi_{zy}\epsilon_{yz} - \mu_{yy}\epsilon_{yz}\epsilon_{zy} + \zeta_{yz}\xi_{yy}\epsilon_{zy} - \zeta_{yy}\xi_{yy}\epsilon_{zz} & \zeta_{yy}\xi_{zy}\epsilon_{yx} - \mu_{yy}\epsilon_{yx}\epsilon_{zy} - \zeta_{yx}\xi_{zy}\epsilon_{yy} + \mu_{yy}\epsilon_{yy}\epsilon_{zx} - \zeta_{yy}\xi_{yy}\epsilon_{zx} + \zeta_{yx}\xi_{yy}\epsilon_{zy} \end{pmatrix}$$

$$\begin{pmatrix} -\zeta_{xy}\mu_{yy}\xi_{yz} + \zeta_{xy}\mu_{yz}\xi_{yy} + \zeta_{yy}\mu_{xy}\xi_{yz} - \zeta_{yy}\mu_{xz}\xi_{yy} - \mu_{xy}\mu_{yz}\epsilon_{yy} + \mu_{xz}\mu_{yy}\epsilon_{yy} & \zeta_{xy}\mu_{yx}\xi_{yy} - \zeta_{xy}\mu_{yy}\xi_{yx} - \zeta_{yy}\mu_{xx}\xi_{yy} + \zeta_{yy}\mu_{xy}\xi_{yx} + \mu_{xx}\mu_{yy}\epsilon_{yy} - \mu_{xy}\mu_{yx}\epsilon_{yy} \\ -\zeta_{yy}\mu_{zy}\xi_{yz} + \zeta_{yy}\mu_{zz}\xi_{yy} + \zeta_{zy}\mu_{yy}\xi_{yz} - \zeta_{zy}\mu_{yz}\xi_{yy} - \mu_{yy}\mu_{zz}\epsilon_{yy} + \mu_{yz}\mu_{zy}\epsilon_{yy} & \zeta_{yy}\mu_{zx}\xi_{yy} - \zeta_{yy}\mu_{zy}\xi_{yx} - \zeta_{zy}\mu_{yx}\xi_{yy} + \zeta_{zy}\mu_{yy}\xi_{yx} + \mu_{yx}\mu_{zy}\epsilon_{yy} - \mu_{yy}\mu_{zx}\epsilon_{yy} \\ -\zeta_{yy}\xi_{xy}\xi_{yz} + \zeta_{yy}\xi_{xz}\xi_{yy} + \mu_{yy}\xi_{yz}\epsilon_{xy} - \mu_{yz}\xi_{yy}\epsilon_{xy} - \mu_{yy}\xi_{xz}\epsilon_{yy} + \mu_{yz}\xi_{xy}\epsilon_{yy} & \zeta_{yy}\xi_{xx}\xi_{yy} - \zeta_{yy}\xi_{xy}\xi_{yx} - \mu_{yx}\xi_{yy}\epsilon_{xy} + \mu_{yy}\xi_{yx}\epsilon_{xy} + \mu_{yx}\xi_{xy}\epsilon_{yy} - \mu_{yy}\xi_{xx}\epsilon_{yy} \\ -\zeta_{yy}\xi_{yy}\xi_{zz} + \zeta_{yy}\xi_{yz}\xi_{zy} + \mu_{yy}\xi_{zz}\epsilon_{yy} - \mu_{yz}\xi_{zy}\epsilon_{yy} - \mu_{yy}\xi_{yz}\epsilon_{zy} + \mu_{yz}\xi_{yy}\epsilon_{zy} & \zeta_{yy}\xi_{yx}\xi_{zy} - \zeta_{yy}\xi_{yy}\xi_{zx} - \mu_{yx}\xi_{zy}\epsilon_{yy} + \mu_{yy}\xi_{zx}\epsilon_{yy} + \mu_{yx}\xi_{yy}\epsilon_{zy} - \mu_{yy}\xi_{yx}\epsilon_{zy} \end{pmatrix} \tag{A3}$$

$$\boldsymbol{M}_{yo}^{(1)} = \begin{pmatrix} \zeta_{yz}\xi_{yy} - \mu_{yy}\epsilon_{yz} & \xi_{yy}(\zeta_{yx} - \zeta_{xy}) - \mu_{yy}\epsilon_{yx} + \mu_{xy}\epsilon_{yy} & \mu_{yz}\xi_{yy} - \mu_{yy}\xi_{yz} & -\mu_{yy}(\zeta_{xy} + \xi_{yx}) + \zeta_{yy}\mu_{xy} + \mu_{yx}\xi_{yy} \\ 0 & \zeta_{zy}\xi_{yy} - \mu_{zy}\epsilon_{yy} & 0 & \zeta_{zy}\mu_{yy} - \zeta_{yy}\mu_{zy} \\ \zeta_{yy}\epsilon_{yz} - \zeta_{yz}\epsilon_{yy} & \xi_{yy}\epsilon_{yx} + \zeta_{yy}\epsilon_{yx} - \epsilon_{yy}(\zeta_{yx} + \xi_{xy}) & \zeta_{yy}\xi_{yz} - \mu_{yz}\epsilon_{yy} & \zeta_{yy}(\xi_{yx} - \xi_{xy}) + \mu_{yy}\epsilon_{xy} + \mu_{yx}(-\epsilon_{yy}) \\ 0 & \xi_{zy}\epsilon_{yy} - \xi_{yy}\epsilon_{zy} & 0 & \zeta_{yy}\xi_{zy} - \mu_{yy}\epsilon_{zy} \end{pmatrix} \tag{A4}$$

$$\boldsymbol{M}_{yo}^{(2)} = \begin{pmatrix} 0 & -\xi_{yy} & 0 & -\mu yy \\ 0 & 0 & 0 & 0 \\ 0 & \epsilon_{yy} & 0 & \zeta_{yy} \\ 0 & 0 & 0 & 0 \end{pmatrix} \tag{A5}$$

$$\boldsymbol{M}_{y1} = \frac{\boldsymbol{M}_{y1}^{(0)} + \alpha_o \boldsymbol{M}_{y1}^{(1)}/\omega}{\epsilon_{yy}\mu_{yy} - \zeta_{yy}\xi_{yy}} \tag{A6}$$

$$\boldsymbol{M}_{y1}^{(0)} = \begin{pmatrix} \mu_{xy}\epsilon_{yy} - \zeta_{xy}\xi_{yy} & 0 & \zeta_{yy}\mu_{xy} - \zeta_{xy}\mu_{yy} & 0 \\ -\zeta_{yz}\xi_{yy} + \zeta_{zy}\xi_{yy} - \mu_{zy}\epsilon_{yy} + \mu_{yy}\epsilon_{yz} & \mu_{yy}\epsilon_{yx} - \zeta_{yx}\xi_{yy} & -\zeta_{yy}\mu_{zy} + \zeta_{zy}\mu_{yy} + \mu_{yy}\xi_{yz} - \mu_{yz}\xi_{yy} & \mu_{yy}\xi_{yx} - \mu_{yx}\xi_{yy} \\ \xi_{yy}\epsilon_{xy} - \xi_{xy}\epsilon_{yy} & 0 & \mu_{yy}\epsilon_{xy} - \zeta_{yy}\xi_{xy} & 0 \\ \zeta_{yz}\epsilon_{yy} + \xi_{zy}\epsilon_{yy} + \zeta_{yy}(-\epsilon_{yz}) - \xi_{yy}\epsilon_{zy} & \zeta_{yx}\epsilon_{yy} - \zeta_{yy}\epsilon_{yx} & -\zeta_{yy}\xi_{yz} + \zeta_{yy}\xi_{zy} + \mu_{yz}\epsilon_{yy} + \mu_{yy}(-\epsilon_{zy}) & \mu_{yx}\epsilon_{yy} - \zeta_{yy}\xi_{yx} \end{pmatrix} \tag{A7}$$

$$\boldsymbol{M}_{y1}^{(1)} = \begin{pmatrix} -\xi_{yy} & 0 & -\mu_{yy} & 0 \\ 0 & \xi_{yy} & 0 & \mu_{yy} \\ \epsilon_{yy} & 0 & \zeta_{yy} & 0 \\ 0 & -\epsilon_{yy} & 0 & -\zeta_{yy} \end{pmatrix} \tag{A8}$$

$$\boldsymbol{M}_{y2} = \begin{pmatrix} 0 & 0 & 0 & 0 \\ -\xi_{yy} & 0 & -\mu_{yy} & 0 \\ 0 & 0 & 0 & 0 \\ \epsilon_{yy} & 0 & \zeta_{yy} & 0 \end{pmatrix} \tag{A9}$$

We note that the expressions of $\boldsymbol{M}_{yo}, \boldsymbol{M}_{y1}, \boldsymbol{M}_{y2}$ reported in (A2), (A6), and (A9), respectively, when in factorized form with respect to α_o, allow for immediate evaluation in the case of normal incidence $\alpha_o = 0$ by nullifying the contribution of $\boldsymbol{M}_{yo}^{(1)}, \boldsymbol{M}_{yo}^{(2)}, \boldsymbol{M}_{y1}^{(1)}$ in (A2) and (A6).

References

1. Malyuzhinets, G. Excitation, reflection and emission of surface waves from a wedge with given face impedances. *Sov. Phys.-Dokl.* **1958**, *3*, 752–755.
2. Budaev, B.V. *Diffraction by Wedges*; Number 322 in Pitman Research Notes in Mathematics Series; Longman Scientific & Technical: Harlow, UK, 1995.
3. Senior, T.B.A.; Volakis, J.L. *Approximate Boundary Conditions in Electromagnetics*; Number 41 in IEE Electromagnetic Waves Series; Institution of Electrical Engineers: London, UK, 1995.
4. Osipov, A.V.; Norris, A.N. The Malyuzhinets theory for scattering from wedge boundaries: A review. *Wave Motion* **1999**, *29*, 313–340. https://doi.org/10.1016/S0165-2125(98)00042-0.
5. Babich, V.M.; Lyalinov, M.A.; Grikurov, V.E. *Diffraction Theory: The Sommerfeld-Malyuzhinets Technique*; Alpha Science International: Oxford, UK, 2008.
6. Lyalinov, M.A.; Zhu, N.Y. *Scattering of Wedges and Cones with Impedance Boundary Conditions*; Mario Boella Series on Electromagnetism in Information and Communication Series; SciTech Publishing: Raleigh, NC, USA, 2013.
7. Oberhettinger, F. Diffraction of waves by a wedge. *Commun. Pure Appl. Math.* **1954**, *7*, 551–563. https://doi.org/10.1002/cpa.3160070306.
8. Osipov, A.V. On the method of Kontorovich–Lebedev's integrals for the problems of diffraction in sectorial media. In *Problems of Diffraction and Propagation of Waves*; St Petersburg University Publications: Saint Petersburg, Russia, 1993; Volume 25, pp. 173–219.
9. Rawlins, A.D. Diffraction by, or Diffusion into, a Penetrable Wedge. *Proc. Math. Phys. Eng. Sci.* **1999**, *455*, 2655–2686.
10. Salem, M.A.; Kamel, A.H.; Osipov, A.V. Electromagnetic fields in the presence of an infinite dielectric wedge. *Proc. R. Soc. A Math. Phys. Eng. Sci.* **2006**, *462*, 2503–2522. https://doi.org/10.1098/rspa.2006.1691.
11. Daniele, V.G.; Lombardi, G. *Scattering and Diffraction by Wedges 1: The Wiener-Hopf Solution—Theory*; John Wiley & Sons: Hoboken, NJ, USA, 2020.
12. Daniele, V.G.; Lombardi, G. *Scattering and Diffraction by Wedges 2: The Wiener-Hopf Solution Advanced Applications*; John Wiley & Sons: Hoboken, NJ, USA, 2020. https://doi.org/10.1002/9781119779452.
13. Daniele, V.G.; Lombardi, G.; Zich, R.S. Network representations of angular regions for electromagnetic scattering. *PLoS ONE* **2017**, *12*, e0182763. https://doi.org/10.1371/journal.pone.0182763.
14. Sommerfeld, A. Mathematische Theorie der Diffraction. *Math. Ann.* **1896**, *47*, 317–374. https://doi.org/10.1007/BF01447273.
15. Seshadri, S.; Rajagopal, A. Diffraction by a perfectly conducting semi-infinite screen in an anisotropic plasma. *IEEE Trans. Antennas Propag.* **1963**, *11*, 497–502. https://doi.org/10.1109/TAP.1963.1138071.
16. Jull, E.V. Diffraction by a conducting half-plane in an anisotropic plasma. *Can. J. Phys.* **1964**, *42*, 1455–1468. https://doi.org/10.1139/p64-133.
17. Felsen, L.B. Propagation and diffraction in uniaxially anisotropic regions. Part 1. Theory. *Proc. Inst. Electr. Eng.* **1964**, *111*, 445–453. https://doi.org/10.1049/piee.1964.0081.
18. Felsen, L.B. Propagation and diffraction in uniaxially anisotropic regions. Part 2. Applications. *Proc. Inst. Electr. Eng.* **1964**, *111*, 454–464. https://doi.org/10.1049/piee.1964.0082.
19. Williams, W.E. Electromagnetic Diffraction in an Anisotropic Medium. *IMA J. Appl. Math.* **1966**, *2*, 186–196. https://doi.org/10.1093/imamat/2.2.186.
20. Hurd, R.A.; Przeździecki, S. Diffraction by a half-plane perpendicular to the distinguished axis of a gyrotropic medium. *J. Math. Phys.* **1976**, *17*, 1838–1847. https://doi.org/10.1063/1.522804.
21. Przedziecki, S.; Hurd, R.A. Diffraction by a half-plane perpendicular to the distinguished axis of a general gyrotropic medium. *Can. J. Phys.* **1977**, *55*, 305–324. https://doi.org/10.1139/p77-045.
22. Hurd, R.; Przedziecki, S. Half-plane diffraction in a gyrotropic medium. *IEEE Trans. Antennas Propag.* **1985**, *33*, 813–822. https://doi.org/10.1109/TAP.1985.1143679.
23. Przedziecki, S. Half-plane diffraction in a chiral medium. *Wave Motion* **2000**, *32*, 157–200. https://doi.org/10.1016/S0165-2125(00)00037-8.
24. Daniele, V.; Graglia, R.D. Diffraction by an imperfect half plane in a bianisotropic medium. *Radio Sci.* **2007**, *42*, 1–16. https://doi.org/10.1029/2007RS003674.
25. Tellegen, B.D. The gyrator, a new electric network element. *Philips Res. Rep* **1948**, *3*, 81–101.
26. Cheng, D.; Kong, J.A. Covariant descriptions of bianisotropic media. *Proc. IEEE* **1968**, *56*, 248–251. https://doi.org/10.1109/PROC.1968.6268.
27. Lindell, I.; Sihvola, A.; Tretyakov, S.; Viitanen, A.J. *Electromagnetic Waves in Chiral and Bi-Isotropic Media*; Antennas and Propagation Library, Artech House: Boston, MA, USA, 1994.

28. Olyslager, F. The behavior of electromagnetic fields at edges in bi-isotropic and bi-anisotropic materials. *IEEE Trans. Antennas Propag.* **1994**, *42*, 1392–1397. https://doi.org/10.1109/8.320745.
29. Vashtalov, S.; Fisanov, V. Diffraction of a plane wave from a wedge in a chiral medium. *Russ. Phys. J.* **1993**, *36*, 982–989.
30. Daniele, V.G.; Lombardi, G.; Zich, R.S. The Electromagnetic Field for a PEC Wedge Over a Grounded Dielectric Slab: 2. Diffraction, Modal Field, Surface Waves, and Leaky Waves. *Radio Sci.* **2017**, *52*, 1492–1509. https://doi.org/10.1002/2017RS006388.
31. Daniele, V.; Lombardi, G.; Zich, R.S. The Double PEC Wedge Problem: Diffraction and Total Far Field. *IEEE Trans. Antennas Propag.* **2018**, *66*, 6482–6499. https://doi.org/10.1109/TAP.2018.2877260.
32. Daniele, V.; Lombardi, G.; Zich, R.S. Radiation and Scattering of an Arbitrarily Flanged Dielectric-Loaded Waveguide. *IEEE Trans. Antennas Propag.* **2019**, *67*, 7569–7584. https://doi.org/10.1109/TAP.2019.2948494.
33. Daniele, V.G.; Zich, R.S. *The Wiener-Hopf Method in Electromagnetics*; Mario Boella Series on Electromagnetism in Information and Communication Series; SciTech Publishing: Raleigh, NC, USA, 2014.
34. Daniele, V.G.; Lombardi, G. The generalized Wiener–Hopf equations for wave motion in angular regions: Electromagnetic application. *Proc. R. Soc. A Math. Phys. Eng. Sci.* **2021**, *477*, 20210040. https://doi.org/10.1098/rspa.2021.0040.
35. Bresler A.D.; Marcuvitz, N. *Operator Methods in Electromagnetic Field Theory*; Report R-495,56, PIB425; MRI Polytechnic Institute of Brooklyn: New York, NY, USA, 1956.
36. Felsen, L.B.; Marcuvitz, N. *Radiation and Scattering of Waves*; Prentice-Hall: Englewood Cliffs, NJ, USA, 1973.
37. Daniele, V.G.; Zich, R.S. Radiation by arbitrary sources in anisotropic stratified media. *Radio Sci.* **1973**, *8*, 63–70. https://doi.org/10.1029/RS008i001p00063.
38. Noble, B. *Methods Based on the Wiener-Hopf Technique for the Solution of Partial Differential Equations*; Pergamon Press: London, UK, 1958.
39. DeRusso, P.; Roy, R.; Charles, M. *State Variables for Engineers*; Wiley: New York, NY, USA, 1965.
40. Lombardi, G. Skew Incidence on Concave Wedge With Anisotropic Surface Impedance. *IEEE Antennas Wirel. Propag. Lett.* **2012**, *11*, 1141–1145. https://doi.org/10.1109/LAWP.2012.2219845.
41. Kantorovich, L.V. *Approximate Methods of Higher Analysis*; Noordhoff: Groningen, The Netherlands, 1958.
42. Lombardi, G.; Papapicco, D. Quadrature of functions with endpoint singular and generalised polynomial behaviour in computational physics. *Comput. Phys. Commun.* **2024**, *299*, 109124. https://doi.org/10.1016/j.cpc.2024.109124.